Investigation of *mlh-3* & *mlh-1* in *C. elegans*

by

Asier Bracho

BS in Biology, Florida International University, 2018

Submitted to the Graduate Faculty of the

School of Public Health in partial fulfillment

of the requirements for the degree of

Master of Science

University of Pittsburgh

2023

UNIVERSITY OF PITTSBURGH

SCHOOL OF PUBLIC HEALTH

This thesis was presented

by

Asier Bracho

It was defended on

April 17, 2023

and approved by

Judith L. Yanowitz, PhD (Thesis Advisor, Committee Chair), Professor, Department of OB/GYN/RS

Beth L. Roman, PhD, Associate Professor, Department of Human Genetics

Quasar Padiath, PhD, Associate Professor, Department of Human Genetics

Investigation of *mlh-3* & *mlh-1* in *C. elegans*

Asier Bracho, MS

University of Pittsburgh, 2023

Mlh1 and *Mlh3* are genes found in mammals with roles in meiosis and DNA mismatch repair. Their protein products function as heterodimers that resolve double-Holliday junctions during meiosis I. In mammals, knockouts of both genes result in infertile mice, while in *C. elegans,* homozygous knockouts of *mlh-1* appear viable. We identified the *C. elegans* gene *ZK1098.3* as a possible *Mlh3* homolog due to the similar predicted functions in their products. We hypothesize that *ZK1098.3* is the *C. elegans* homolog of *Mlh3* (*mlh-3),* and that it, together with *mlh-1,* may be functioning to repair non-canonical COs. We procured or produced knockouts of both genes and crossed them into meiotically sensitive backgrounds. We also tagged ZK1098.3 with V5. Our results showed localization of ZK1098.3 protein in the meiotic portion of the worm germ line, supporting the hypothesis that this gene is involved in meiosis. One of the *mlh-1* KOs produced extra DAPI bodies in diakinesis and showed slow growth. However, the other *mlh-1* KO, along with the *mlh-3* KOs and various crosses into sensitized backgrounds, appeared phenotypically normal. This leads us to the conclusion that while *mlh-1* and *ZK1098.3* may have roles in meiosis, they are only minor, and further work is necessary to understand their functions.

Table of Contents

List of Tables

List of Figures

Preface

Acknowledgments

I would like to express my gratitude to Judith L. Yanowitz, my thesis advisor, for readily accepting me into her lab, and for all her guidance, feedback, and encouragement. Major thanks go out to the other members of my committee for all their advice, both specific to my project and in broader academic and career pursuits. My thanks and acknowledgements to Marilina Raices and Michelle L. Scuzzarella, specifically for confocal imaging of antibody staining and injection of germ lines with CRISPR/Cas9, respectively. But also, my undying gratitude for their never-ending patience with me as I continued to learn my way around the lab. Thank you to my parents for every ounce of work they put in for me, and to Aitor, Kathryn and Robert, for their unceasing check-ins and support. To my fellow grad school friends from orientation day 1, thank you for being there every weekend and letting me vent. A todos los amigos y familiares que me ayudaron, mucho cariño y muchas gracias.

1.0 Background

Meiosis is an integral process for fertility. It produces haploid daughter cells for use in fertilization and zygote formation. This is achieved partly through homologous chromosome segregation, occurring in the first anaphase of meiosis. Appropriate segregation of homologous chromosomes requires their proper alignment on the meiotic spindle. Crossing over helps accomplish this alignment by firmly binding together homologous chromosomes. If crossing over does not occur faithfully, homologous chromosomes may not align or segregate properly. This missegregation can cause aneuploidy, which can induce fertility problems (Gruhn *et al*., 2019).

Crossovers (COs) are accomplished by the intentional formation of double-strand breaks (DSBs) (Figure 1). The broken ends are resected to produce overhanging single stranded DNA ends. Through homology, one strand will invade the adjacent (and unbroken) homologous chromosome, to form a D-loop where DNA end extension begins. The resulting chromosomal intermediates eventually form double Holliday junctions (dHJs) which must be cleaved (or resolved) before the completion of Meiosis I. In mammals, the Mlh1/Mlh3 heterodimer is used to achieve this resolution. Mlh3 acts as a 3' to 5' exonuclease to cleave Holliday junctions, while Mlh1 acts in mismatch repair and is essential for Mlh3 to properly function (Dai *et al*., 2021). *Mlh3* and *Mlh1* mouse knockouts (KOs) show a decrease in crossing over and an increase in aneuploidy (Eaker *et al*., 2002 and Lipkin *et al*., 2002). Mutations in *MLH1* and *MLH3* in humans are associated with several disorders, including infertility (Singh *et al*., 2021).

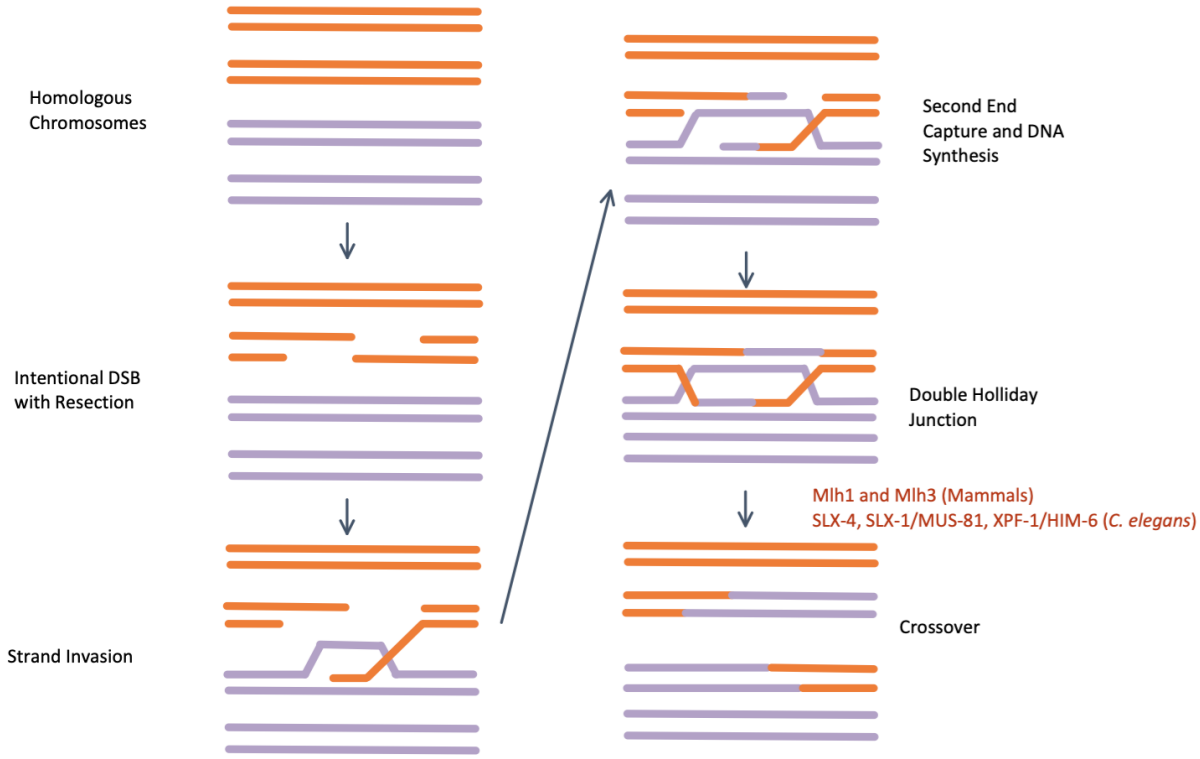

Figure 1: Double Holliday Junction Formation and Crossovers

Crossover formation steps depicting a double Holliday junction. The red indicates the proteins used to resolve dHJs in mammals and *C. elegans.* Made with information from Hillers *et al.*, 2017.

C. elegans is a useful model organism for studying meiosis due to its clearly visible germ line, with easily identifiable stages of meiosis using DAPI staining (Figure 2). The germ line forms an easy-to-follow path from the mitotic tip into meiotic prophase I stages, starting with the leptotene and ending with diakinesis in the oocytes just before the spermatheca (Hillers *et al.*, 2017). The individual oocytes are readily observable, and adjacent to the spermatheca (indicated by the presence of a cluster of spermatocytes), the -1 and -2 oocytes can be easily identified. At this stage, homologous chromosomes are visible as DAPI bodies. In wild-type worms, there are 6 bivalent DAPI bodies, one for each homologous chromosome pair, bound together by chiasmata

(Hillers *et al*., 2017). Thus, errors in crossing over are apparent in the form of abnormal DAPI body counts, representing fusions (<5 DAPI bodies) or univalent chromosomes (>6 DAPI bodies). Sex in *C. elegans* is determined by the presence of two X chromosomes (hermaphrodite) or one X chromosome (male, product of nondisjunction) (Herman, 2005). Males can be characterized by their distinctive blunt or hook-shaped tail (Emmons, 2005). Meiotic mutants increase the percentage of males in the populations since they arise from nondisjunction of an X chromosome during meiosis.

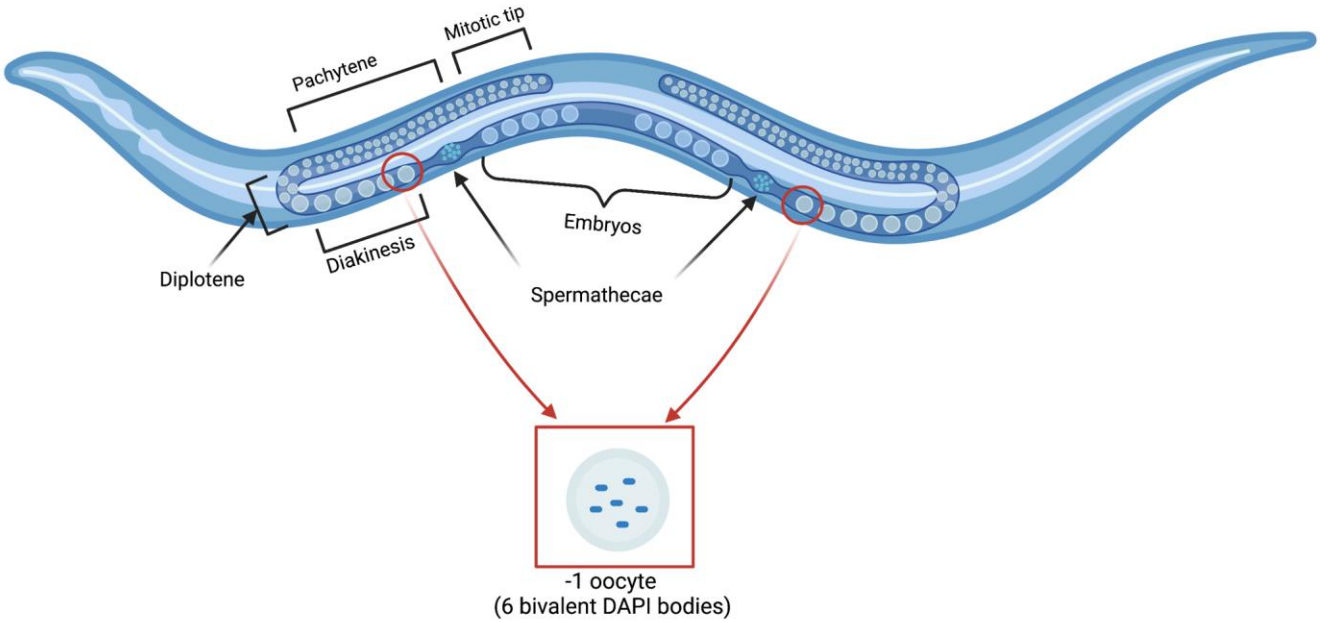

Figure 2: *C. elegans* Germ Lines

Made using information from Hillers *et al*., 2017. Created with BioRender.com.

Mlh1 and Mlh3 are conserved between mice, yeast, and humans, yet they do not appear to play a similarly central role in worm meiosis. Resolution of dHJs in wild-type *C. elegans* appears to take place primarily via SLX-4, SLX-1/ MUS-81, and XPF-1/HIM-6 complexes (Hillers *et al*., 2017). The *C. elegans Mlh1* homolog *mlh-1* was identified via RNAi screening (Tijsterman *et al*., 2002). An *Mlh3* homolog, however, has not been officially recognized, but the gene *ZK1098.3* was identified by our group as a putative candidate based on its predicted protein function rather than by alignment. It was identified via a search on WormBase for uncharacterized 3' to 5' exonucleases in *C. elegans.* Worm *mlh-1* and putative *mlh-3* knockouts appear viable. Resolved dHJs in this model organism are marked by the protein COSA-1 (Yokoo *et al*., 2012). COSA-1 binds chromosomes at CO sites, and acts as a reinforcement mechanism for CO formation. It is an ortholog of CNTD1 in mice/humans (Yokoo *et al*., 2012).

This project focuses on understanding the function of the MLH-1 and MLH-3 proteins in *C. elegans*. Under normal conditions in wild-type *C. elegans*, there is usually one CO per chromosome (Hillers *et al*., 2017), considered and referred to here as the canonical CO. This is in stark contrast to other species, which can vary in the number of COs per chromosome that they experience in meiosis (Martinez-Perez and Colaiacovo, 2009). Under stressful conditions such as heat, radiation, or in certain genetic backgrounds, there may be excess or fewer COs per chromosome (more or less than one). These excess COs are herein referred to as "noncanonical" and make up no more than 35% of autosomal COs in wild-type worms (Hillers *et al*., 2017 and Lim, Stine and Yanowitz, 2008). They may not be marked by COSA-1 (Yokoo *et al*., 2012), making them distinguishable from the canonical COs. In other species, mechanisms exist for preventing excess dHJs between homologs, such as Sgs1 in yeast (Oh *et al*., 2007). Here we hypothesize that, in *C. elegans*, MLH-1 and MLH-3 are used in a separate pathway not involving

COSA-1 to repair noncanonical COs. Two abnormal CO backgrounds, used in this project, are *him-5* and *msh-5*. Knockouts of the *him-5* gene cause a failure in crossover formation (and thus nondisjunction) of the X chromosome, leading 7 DAPI bodies in the diakinesis oocytes and to a high incidence of male progeny (Hodgkin, Horvitz and Brenner, 1979). The *msh-5*(*ea36*) allele has a mild phenotype of producing fewer than six crossovers, leading to an occasional 7 DAPI bodies at diakinesis (Macaisne at al., 2022).

1.1 Specific Aims

1.1.1 Aim 1

This project's first aim is to test the hypothesis that *ZK1098.3* in *C. elegans* is the homolog of mammalian *Mlh3*. *C. elegans* currently has no accepted homolog for Mlh3. This protein functions as a heterodimer with Mlh1, and *C. elegans* has an Mlh1 homolog. I attempted to use yeast two hybrid assays to test whether ZK1098.3 is interacting with MLH-1. Furthermore, I assessed ZK1098.3 localization by addition of a V5 tag to the gene and using immunohistochemistry to visualize the proteins using confocal microscopy.

1.1.2 Aim 2

The second hypothesis being tested is that MLH-3 and MLH-1 in *C. elegans* function to resolve noncanonical COs. By producing *mlh-3* and *mlh-1* knockout (KO) worms and exposing them to conditions and genetic backgrounds where noncanonical COs occur, we reasoned that a

phenotype would be observed. We expected that in the absence of the *mlh-1* and *mlh-3* genes, noncanonical COs will not be resolved, leading to meiotic defects. These defects could be observed by the appearance of abnormal DAPI body numbers, with 6 being normal in most backgrounds. I visualized and quantified the number of DAPI bodies using confocal microscopy.

1.2 Public Health Impact of this Work

Infertility affects 1 out of every 6 people (World Health Organization, 2023), putting a significant burden on families attempting to conceive. Errors in meiosis can be at fault for infertility (Gruhn *et al*., 2019). The various causes of meiotic errors are not yet fully understood. *C. elegans* is an important model organism for several processes, including meiosis. Homologs of human genes can be readily identified in this worm. The shape of their germ line allows for each stage of meiosis to be observed sequentially (Figure 2), and mutants can be generated in much shorter time intervals than in model organisms such as mice. This allows for rapid analysis of genetic variants that may be associated with infertility, provided that the variants exist in a human gene with a *C. elegans* homolog. Identifying the homolog of Mlh3 and the function of both Mlh1 and Mlh3 homologs would strengthen our collective knowledge on *C. elegans* meiosis, as well as provide more opportunities to study variants of these genes and their functions. This could provide a pathway to more treatments for infertility.

2.0 Methods

2.1 Maintaining Stocks

All worms were maintained on 6 cm MYOB (Modified Youngren's, Only Bacto-peptone) plates, seeded with OP50. Worms were picked and replated twice a week at the L4 stage to avoid starvation, and kept in an incubator at 20° or 25° C. The formula for MYOB is as follows:

2g NaCl

0.55g TrisHCl

0.24g TrisOH

4.6g Bactotryptone

5 mg Cholesterol

20g Agar

1L Water

Thoroughly mixed and autoclaved.

2.2 Stocks

Knockouts of *mlh-1* were procured from the *Caenorhabditis* Genome Center (CGC). Two alleles were obtained: *ok1917* and *gk516* (*C. elegans* Deletion Mutant Consortium, 2012). The *ok1917* allele was used for most crosses in the following sections, as it appeared at first to be a healthy stock with no visible phenotypes besides the production of males. The *gk516* stock

displayed an uncoordinated phenotype. The details for both the *ok1917* and *gk516* KOs can be found in Figure 1.

Knockouts for *ZK1098.3* were produced in our laboratory by Michelle Scuzzarella using CRISPR/Cas9. The knockouts were successful in five parental lines, labeled as *ea99, ea100, ea101,* 833.11 and 833.13. The latter two were balanced with *qC1* and maintained as a balancer heterozygous stock, while *ea101* was balanced in the same way but crossed into a *him-5* background. The *him-5* knockout allele (*ea42*) was produced by Nicolas Macaisne, Zebulin Kessler and Judith L. Yanowitz (Macaisne, Kessler and Yanowitz, 2018). The *msh-5(ea36)* V allele was produced by Judith L. Yanowitz by CRISPR and is a weak loss-of-function of this locus. The *msh-5* strain is marked with *dpy-1(e1) III* to facilitate crosses (Macaisne at al., 2022). *dpy-1* confers a dumpy (Dpy) phenotype when homozygous and a normal, full-length animal when heterozygous. The presence of normal animals on a plate with a Dpy parent would indicate a successful mating. All other stocks were produced by crosses or via CRISPR injection. A stock with the transheterozygous balancers *qC1/hT2* was utilized to obtain balanced mutations on chromosome III. All crosses were carried out on 3cm MYOB plates freshly seeded with OP50 bacteria.

2.2.1 Generation of *mlh-1;mlh-3;msh-5;him-5* Quadruple Mutant and *mlh-3;msh-5;him-5* Triple Mutant

This cross was attempted multiple times. Each time, five sets of crosses were set up with 2 *mlh-3(ea101);him-5(ea42)* L4 hermaphrodite worms and 5-7 *mlh-1(ok1917)* males. Males from the F1 generation, all of which are heterozygous for each mutation, were then crossed with *qC1/hT2* hermaphrodites (which show a rolling (Rol) and GFP-positive phenotype). This was done

to isolate and balance a chromosome(s) with *mlh-1* and *ZK1098.3* KO alleles on it, as these genes are linked, situated approximately 21 cM apart on chromosome III. Given the expected recombination frequency (21%, with half being the desired recombinant), 40 F2 offspring were collected and individually plated from each set of crosses. We selected non-rolling worms with a GFP^+ green pharynx, indicating a successful cross, and offspring that are balanced by *hT2 III*. Despite repeating this cross three times, genotyping by PCR failed to identify a single offspring with all mutations.

In the third iteration of this cross, the males from the F1 generation were also used to produce *mlh-3(ea101);msh-5(ea36);him-5(ea42)* and *mlh-1(ok1917);msh-5(ea36)* double mutant stocks. The F1 *mlh-1/mlh-3* males were crossed with *dpy-1(e1);msh-5(ea36)* L4 hermaphrodites at a ratio of 2 hermaphrodites to 4-5 males. Therefore, non-Dpy progeny indicated a successful cross. The non-Dpy offspring (F2) were individually plated and genotyped using PCR. While this cross failed to produce an *mlh-1;msh-5* stock, a *mlh-3;msh-5;him-5* stock was successfully generated. Fortuitously, two plates also genotyped positive for all three alleles (*msh-5*, *mlh-3* and *mlh-1*) suggesting *mlh-1* and *mlh-3* had recombined onto the same chromosome in the sperm. We individually plated subsequent generations to obtain a mutant that is homozygous for all alleles, arriving at a quadruple mutant (*mlh-3(ea101);mlh-1(ok1917);msh-5(ea36);him-5(ea42)*).

2.2.2 Generation of *mlh-1;msh-5* Double Mutant

Since the initial attempt to make this double mutant failed, we attempted a separate cross to produce *mlh-1;msh-5* double mutants. Five plates with four or more males from the *mlh-1(ok1917)* stock were plated with two *dpy-1(e1);msh-5(ea36)* L4 hermaphrodites. The non-Dpy F1 offspring was allowed to self, producing F2. Non-Dpy F2 were then plated individually (8 worms from each

cross plate) to be genotyped using PCR. This cross successfully yielded an *mlh-1(ok1917);msh-5(ea36)* stock.

2.2.3 Outcrossing of *mlh-1*

To investigate the health of the *mlh-1(ok1917)* stock, six to nine males were plated with two wildtype (N2) hermaphrodite L4 worms. The F1 heterozygotes were allowed to self, producing F2s. F2 worms were then plated individually (8 worms from each cross plate) to be genotyped using PCR. This unfortunately failed to yield an *mlh-1(ok1917)* homozygous stock, as all progeny yielded a wild-type phenotype, indicating that the initial *mlh-1* males had failed to mate.

2.2.4 Production of V5 Tag on ZK1098.3

We added a V5 tag to the N-terminus of the ZK1098.3 protein using CRISPR. A PAM site was identified just upstream of the start codon, and the 20 bp on the 5' side were targeted with an sgRNA (Table 4). A repair template containing the V5 tag along with a new start codon was designed with homology arms (about 40 bp upstream and 50 bp downstream) to match both sides of the DSB alongside the cut site. The tag was inserted directly upstream of the original start codon. Injections of 1 day-old adult worm germ lines were carried out by Michelle Scuzzarella. A co-injection marker (*dpy-10*) was used to distinguish offspring that had taken up the injection mix. The *dpy-10* marker yields a Rolling (Rol) phenotype when heterozygous and a Dumpy (Dpy) phenotype when homozygous, making it simple to select for heterozygous offspring that can be allowed to self and yield a homozygous insert without the marker.

Three days post-injection, individual Rol and Dpy offspring (F1) were individually plated. These offspring were allowed to self, and the resulting F2 generation was genotyped. Genotyping was carried out via PCR utilizing a reverse primer within the V5 tag, which was not predicted to bind anywhere else in the *C. elegans* genome. Non-Rol offspring from any plate positive for the insert were replated and allowed to self. Once the non-Rol F2 generation had laid eggs, they were individually genotyped. Homozygous worms were distinguished from heterozygous worms by a larger band when genotyped with wild-type primers (63 bp larger). Worms found to be homozygous were then sequenced using Sanger sequencing on their PCR product (Figure 17). This process successfully produced two alleles with the V5 tag (*ea102* and *ea103*), both of which grow normally and appear wild-type.

2.3 Staining

2.3.1 Whole-Mount DAPI Staining

L4 hermaphrodites were collected and aged 18-24 hours prior to fixation. 10-20 worms (unless otherwise specified) were picked into in 4 µL of M9 buffer on a microscope slide. The M9 buffer was produced as follows (Shaham, 2006):

6 g Na_2HPO_4

3 g KH_2PO_4

5 g NaCl

0.25 g $MgSO_4 \bullet 7H_2O$

1 Liter of water

Thoroughly mixed and autoclaved.

The worms received two 4 µL M9 washes and were then fixed with 10 µL of Carnoy's solution and rapidly rehydrated in 20 µL of DAPI solutions (1% PBS + 0.1% TWEEN + 1:50000 DAPI (starting at 10 mg/mL)). The Carnoy's solution was produced as follows:

150 µL of Acetic Acid

75 µL of Ethanol

25 µL of Chloroform

Slides were then allowed to incubate for at least 10 minutes in a humidity chamber. All solvent was then removed and replaced with 12 µL of Prolong Diamond mounting media with DAPI and covered with a cover slip. All slides were allowed to harden at room temperature in the dark overnight and stored at 4 °C prior to imaging.

2.3.2 V5 Antibody Staining of the Germ Line

Between 15 and 30 worms were placed on a Superfrost Plus charged slide with 4 µL of M9 and a drop of 1 mM levamisole, which is used to paralyze the worms. Once the levamisole had taken effect and the worms were paralyzed, the solvent was removed and replaced with 3.5 µL of Sperm Salts (see below). The worms were then dissected by using a needle to slice either the anterior or posterior end, releasing the germ line. Once 4 to 8 germlines were exposed, 3.5 µL of 2% Triton and 7 µL of 2% paraformaldehyde (all diluted in sperm salts) were added, and the slide was allowed to sit in a humidity chamber for 5 minutes. The sperm salts buffer is made as follows:

50 mM PIPES buffer (pH 7)

25 mM KCl

1 mM $MgSO_4$

45 mM NaCl

2 mM $CaCl_2$

A cover slip was then added, and the slide was frozen for 10 minutes. The cover slip was removed, and the slide was submerged in cold (-20 °C) 100% ethanol for 2 minutes, followed by a wash of 50 µL PBS-Tween (0.1%) + BSA (0.1%) and 10 minutes in a humidity chamber. This was repeated two more times, for a total of three washes of PBST. Following the final wash, 50 µL of the diluted antibodies (in PBST-BSA) were added to the slide, which was then allowed to sit overnight in a humidity chamber at 4° C. The V5 tag monoclonal mouse antibodies were acquired from Thermo Fisher Scientific (Catalog number R960-25). They were diluted to 1:500, while the anti-SYP-1 counterstaining antibodies were diluted to 1:1000.

The following day, three 50 µL PBST 10-minute washes were performed, and the secondary antibodies were added and allowed to sit for 2 hours in a humidity chamber. The two secondary antibodies (anti-mouse Alexa 488 and anti-rabbit Alexa 568) were diluted in PBST + BSA to a final concentration of 1:2000. The slides were washed in 50 µL PBST before adding 20 µL of DAPI diluted in PBST for 10 minutes in the humidity chamber. One more wash of 50 µL PBST was performed, and slides were mounted with 12 µL of Prolong Diamond with DAPI mounting media and covered with a cover slip. All slides were allowed to harden in the dark at room temperature overnight and stored at 4° C.

2.3.3 Confocal Imaging and DAPI Body Counts

All slides were analyzed on a Leica Stellaris 5 confocal microscope. The DAPI staining was analyzed using the Alexa 405 laser. DAPI bodies were counted by taking a Z-stack of the relevant region of the germ line (the spermatheca as well as the -1 and -2 oocytes (those just distal

to spermatheca and the first and second to be matured and fertilized). These Z-stacks were then visualized on a rotatable 3-D model, and the numbers of DAPI bodies (bivalents, univalent, and fusions) in the -1 and -2 oocytes were counted. The antibody staining slides were also imaged on the confocal microscope by taking a Z-Stack using 405 nm for DAPI, 488 nm for mouse secondary antibodies, and 568 nm for rabbit secondary antibodies. Individual germ lines were imaged.

2.4 Genotyping

All worm lysates were prepared using a mixture of 2µL of 20 mg/mL (800 units/mL) Proteinase K for every 100 µL of Lysis Buffer. The Lysis Buffer was prepared as follows:

5 mL 1M Tris (pH 8.3)

10 mL 2.5 M KCl

0.75 mL 1M $MgCl_2$

2.25 mL Tween 20

2.25 mL NP-40

479.75 mL Water

Single-worm lysates were made using 14 µL of buffer per sample. Multi-worm lysates were made using 20 µL, and plate lysates were collected by placing 50 µL of buffer on a tilted plate and collecting the buffer that gathered at the bottom. All lysates were run under LYS1 conditions, found in Table 3.

All genotyping was carried out using 10 µL PCR reactions. The PCR concentrations are listed under Table 1. PCR conditions for different genes are listed in Table 3.

The *msh-5(ea36)* allele is a point mutation (C > G), introducing a cut site for the enzyme BsmB1v2. This allowed for genotyping by digesting the PCR product with the enzyme using the reagents listed in Table 2 and run on the program listed as BSMB1v2 (Table 3). This enzyme cleaves the PCR product if the mutation is present, resulting in 2 smaller bands (roughly 200 and 270 bp) of DNA in the agarose gel. This would differentiate the mutant from the wild type, which would not be cleaved. The product was then mixed with 1.5 µL of loading dye and run alongside a ladder on a 2% agarose gel using ethidium bromide dye. All gels were imaged using a Kodak Gel Logic 212 Imaging System.

2.5 Yeast Two Hybrid Assay

2.5.1 Primer Design and Testing

To examine the possible interaction of MLH-1 and MLH-3, we initiated a yeast two hybrid assay. Primers to amplify the entire *mlh-1* and *mlh-3* genes were designed to be less than 30bp long, end on a cytosine or guanine, and have an annealing temperature less than 72° C but more than 45° C (as predicted by the online NEB Tm Calculator). The forward primers started at the start codon, and the reverse primers ended at the last base pair of the final exon for each gene. These primers then each had a homology arm added outside of the gene meant to hybridize with the ends of the linearized plasmid (all primers written 5' to 3', all homology arms added at the 5' end, Table 2).

These primers were first tested using genomic DNA lysates of wild-type worms using the protocol conditions for Phusion® High-Fidelity PCR Master Mix with HF Buffer (listed in Table

3) and run on a 1% agarose gel. When the resulting bands were of the appropriate size for each gene (roughly 6200 bp and 7200 bp for *mlh-3* and *mlh-1*, respectively), these primers were tested in a similar manner using wild-type cDNA. These tests also confirmed the efficacy of these primers, with bands at the appropriate spliced gene sizes (roughly 2300 bp for both genes). The leftover 20 µL of PCR reaction were purified using a NucleoSpin® Gel and PCR Cleanup Kit. The resulting 30 µL per reaction were measured on a NanoDrop 2000 spectrophotometer to obtain the concentration of DNA (55.4 ng/µL for *mlh-1* and 35.4 ng/µL for *mlh-3*).

2.5.2 Plasmid Production

The resultant PCR products were combined with the linearized plasmids (pGAD and pGBD (James, Halladay & Craig, 1996)) by mixing 4 µL of the insert, 1 µL of the plasmid, and 15 µL of Gibson mix, for a total 20 µL of reaction. This was then run on a thermocycler at 55° C for 15 minutes. The results were 4 plasmids:

pGAD + *mlh-1*

pGAD + *mlh-3*

pGBD + *mlh-1*

pGBD + *mlh-3*

2.5.3 Bacterial Transformation/Collection

Competent DH5α cells were aliquoted at 50 µL per tube for each plasmid solution. The appropriate plasmid was added to each tube of bacteria (0.5 µL). The tubes were then incubated on ice for 30 minutes, then 30 seconds in a 42° C water bath, and another 2 minutes on ice. LB

was added to each tube (200 µL), and the tubes were incubated at 37° C for 45 minutes. The plasmid contained an antibiotic resistance gene, so the bacteria were plated (50 µL per plate) on plates with the appropriate antibiotic, selectively growing the bacteria that took up the plasmid. These plates were incubated overnight at 37° C. The next day, 8 bacterial colonies per plate were individually added to 10 µL of nuclease free water and run on a thermocycler for 10 minutes at 99° C. These makeshift lysates were then used in a PCR reaction (DEL40EXT protocol, Table 3) with primers tailored to the plasmids to determine which colonies had the insert. As of the time of writing, this process has failed to yield a colony positive for any of the plasmids. Therefore, we are concerned that there might be problems with the vectors.

2.6 Methods Tables and Gene Diagrams

Table 1: PCR Reagents

Reagents	100 µM Primers (µL/sample)	10 µM Primers (µL/sample)
Water	3.65	27.5
Forward Primer	0.05	5
Reverse Primer	0.05	5
Lucigen® FailSafe PCR 2X PreMix	5	50
Taq DNA Polymerase	0.25	2.5

Table 2: Restriction Enzyme Reagents

Reagents	µL/sample
Water	3.2
Buffer (NEBuffer™ r3.1)	1.5
Enzyme (BsmB1v2)	0.3
PCR Product	10

Table 3: PCR Protocols

Name	Temperatures (°C)	Times	Genes
DEL40	95	2min	*mlh-3 (KO and wt)*
	95	15s	
	55	30s	
	72	1min	
	Repeat steps 2-4 x40		
	72	5min	
	10	∞	
DEL40EXT	95	2min	Testing bacteria-grown plasmids
	95	15s	
	55	30s	
	72	2min	
	Repeat steps 2-4 x40		
	72	5min	
	10	∞	

DEL40MSH	95 95 55 72 Repeat steps 2-4 x55 72 10	2min 15s 30s 1min 5min ∞	*msh-5 (mut and wt)*
BSMB1v2	55 80 12	20min 40min ∞	*msh-5 mut*
Y32	95 95 51 72 Repeat steps 2-4 x40 72 10	3min 30s 30s 1.5min 10min ∞	*mlh-1 (KO and wt)*
LYS1	65 95 10	1hr 15min ∞	All lysates
Phusion	98 98 Variable annealing	30s 10s 30s	Producing yeast two hybrid inserts

	72 Repeat steps 2-4 x35 72 4	2.5min 10min ∞	*mlh-1 (62° C)* *mlh-3 (51° C)*

Table 4: Primers, sgRNAs and Repair Templates

Name	Sequence (5'-3')	Description
AB-001	ACGTCCGCAGGAGGATCTGC	Reverse primer for V5::*mlh-3* insert
AB-006	gatctatgaatcgtagatacATGGGAGATACA ACATCATCGG	Forward primer for *ZK1098.3* Y2H
AB-007	TGAACTTGCGGGGTTTTTCATTAA CAATTCAATTTAATATAATC	Reverse primer for *ZK1098.3* Y2H
AB-008	gatctatgaatcgtagatacATGGGACTAATC CAACGCC	Forward primer for *mlh-1* Y2H
AB-009	TGAACTTGCGGGGTTTTTCATTAT GTTCCACATCGCTCGAAG	Reverse primer for *mlh-1* Y2H
AB-CR001	taaaaatctttttttaagAT	sgRNA for V5 insert
MLS-018	gaggtggaagagcgggaacac	Forward primer for *mlh-3*
MLS-019	gtagcgaaattacggtacctcatctcg	Reverse primer for *mlh-3* KO

MLS-020	caaccgatacttggcagctaccg	Reverse primer for wt *mlh-3* (V5 genotyping)
MLS-021	CCGCTCCAAAAGCCATCTGAAC	Reverse primer for wt *mlh-3*
MSH5-1F	ACTCGAACGCCGAAGTGAC	Forward primer for *msh-5*
MSH5-1R	TCAACGAAAGAGTTAAAACACGAGA	Reverse primer for *msh-5*
ZK-288	cattctgacagaagtttggaacg	Reverse primer for *mlh-1* KO (*ok1917*)
ZK-289	ctgtcgaaacgggtggcc	Forward primer for *mlh-1* KO (*ok1917*)
ZK-294	CACCTCCCTCTACCATCTCGACT	Reverse primer for wt *mlh-1*
V5 Tag Repair Template	cataaatttgaattattagatataaaaatctttttttaaATGGGTAAGCCTATCCCTAACCCTCTCCTCGGTGTCGATTCTACGTCCGCAGGAGGATCTGCTatgggagatacaacatcatcggaagatgttccggaaaataagcaaaaatc	Repair template to insert V5 in *mlh-3,* used in tandem with AB-CR001

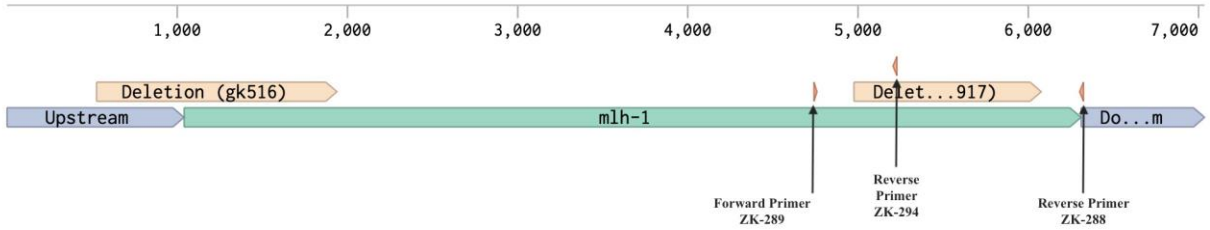

Figure 3: Deletion and Primers for *mlh-1 (ok1917* and *gk516)*

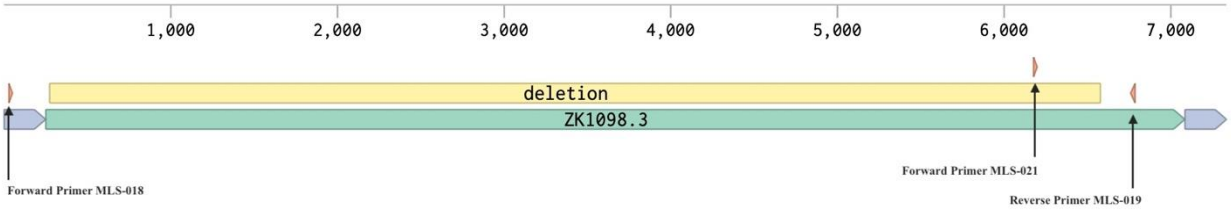

Figure 4: Deletion and Primers for *ZK1098.3* (or *mlh-3*)

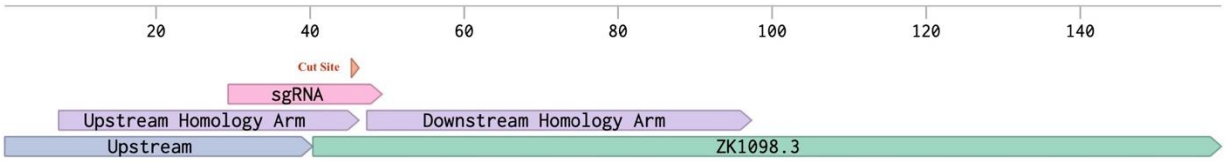

Figure 5: V5 Tagging *ZK1098.3*: sgRNA, Cut Site, and Repair Template Homology Arms

Figure 6: V5 Tagging *ZK1098.3*: Tagged Gene, Genotyping Primers, and Linker

3.0 Results

3.1 Analysis of *mlh-1* and *mlh-3* Phenotypes

To determine the function of the *mlh-1* homolog in worms, two knockouts were obtained from the CGC: *ok1917* and *gk516*. At first glance both stocks seemed healthy, growing at a similar pace as N2 wild-type worms. The *gk516* allele showed a slightly uncoordinated (Unc) phenotype. In case this Unc phenotype was due to some unwanted mutations (as these worms were not characterized as Unc in the CGC website), we decided to focus most of the work for this project on *ok1917*. This stock began presenting male worms over the first few weeks, and these males appeared fertile in trials with *fog-2* worms.

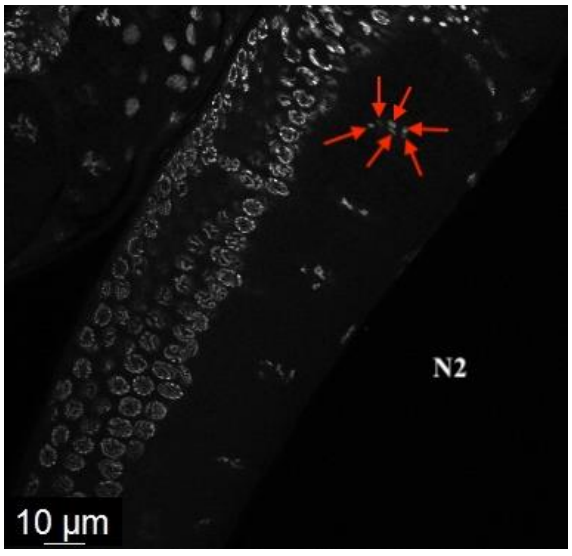

Figure 7: Still image of a DAPI-stained N2 wild-type worm.

This image shows 6 DAPI bodies, two of which appear faint due to varying depths. For this reason, DAPI body counts were obtained (and will be shown) using 3-D models rendered from Z-stacks.

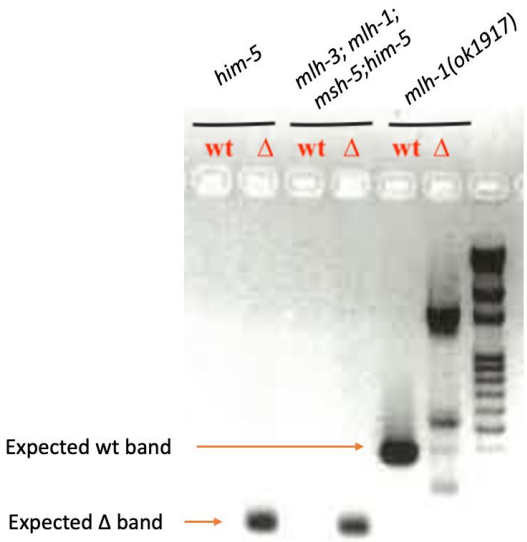

Figure 8: *him-5* PCR Results for *mlh-1(ok1917)* Stock

PCR results showing a *him-5(ea42)* control, the quadruple mutant *mlh-3(ea101);mlh-1(ok1917);msh-5(ea36);him-5(ea42)*, and the *mlh-1(ok1917)* KO. The wt indicates wild type primers and the Δ indicates *ea42* deletion primers. The *him-5* control and the *mlh-3;mlh-1;msh-5;him-5* both show a band for the deletion and no wild-type band, indicating that they are homozygous for *ea42*. The *ok1917* stock shows a wild type band, and no mutant band of the expected size, but there are errant bands.

Over time, the health of this stock appeared to deteriorate. They began growing slowly, as evidenced by the fact that, unlike wild type, these worms would not need to be passed to a new plate twice a week. Crosses attempted later in the project failed, possibly due to the *ok1917* males being too sickly to mate.

Both stocks were stained with DAPI (28 worms for *gk516* and 14 worms for *ok1917*). The *gk516* stock, which appeared to be less healthy early on, had a normal DAPI body count of 6, with no difference detected between the KO and the N2 control (Figures 9-10). By contrast, the *ok1917* stock showed a higher mean DAPI body count at 6.46, which was found to be statistically different

from the control in a Student's t-test with a significance level of 95% (Figure 10). This is consistent with the presentation of males in this stock since males are a product of nondisjunction.

Both stocks were maintained for at least two generations at 25° C to test their response to heat stress. The *gk516* stock was able to grow at a rate comparable to N2 worms at this higher temperature and showed no difference from the control in mean DAPI body count (Figure 14). The *ok1917* stock failed to grow appropriately at the higher temperature. To test whether the presence of males may have been due to contamination with *him-5(ea42)* worms, this stock was genotyped (Figure 8). While this stock showed the appropriate wild-type band with wild-type primers and did not show the accepted *ea42* KO band with mutant primers, there were still some bands present in the mutant lane. Human MLH1 functions in mismatch repair (Bronner *et al*., 1994); therefore it is possible that the *ok1917* homozygous stock has been accumulating mutations over time, leading to these errant bands. If this is the case, it is unclear whether the inability to grow at 25° C is due to the KO itself, or accumulated damage elsewhere in the genome. An outcross of *ok1917* to N2 worms was attempted, with the intention of reproducing the homozygous *mlh-1* KO. However, this cross failed, potentially due to the sickly nature of the stock. Another stock of *mlh-1(ok1917);msh*-5(*ea36*) was produced. The *msh-5*(*ea36*) allele has been shown to produce univalent chromosomes in diakinesis at low frequency, (seen as 7-8 DAPI bodies (Macaisne *et al*., 2022)). This stock showed no statistically significant difference in mean DAPI body count from the *msh-5(ea36)* control (Figure 13). Furthermore, the sickly phenotype of the *ok1917* single mutant was not present in the *mlh-1(ok1917);msh-5(ea36)* double mutant. These data support the presence of a mutation elsewhere in the genome causing this phenotype.

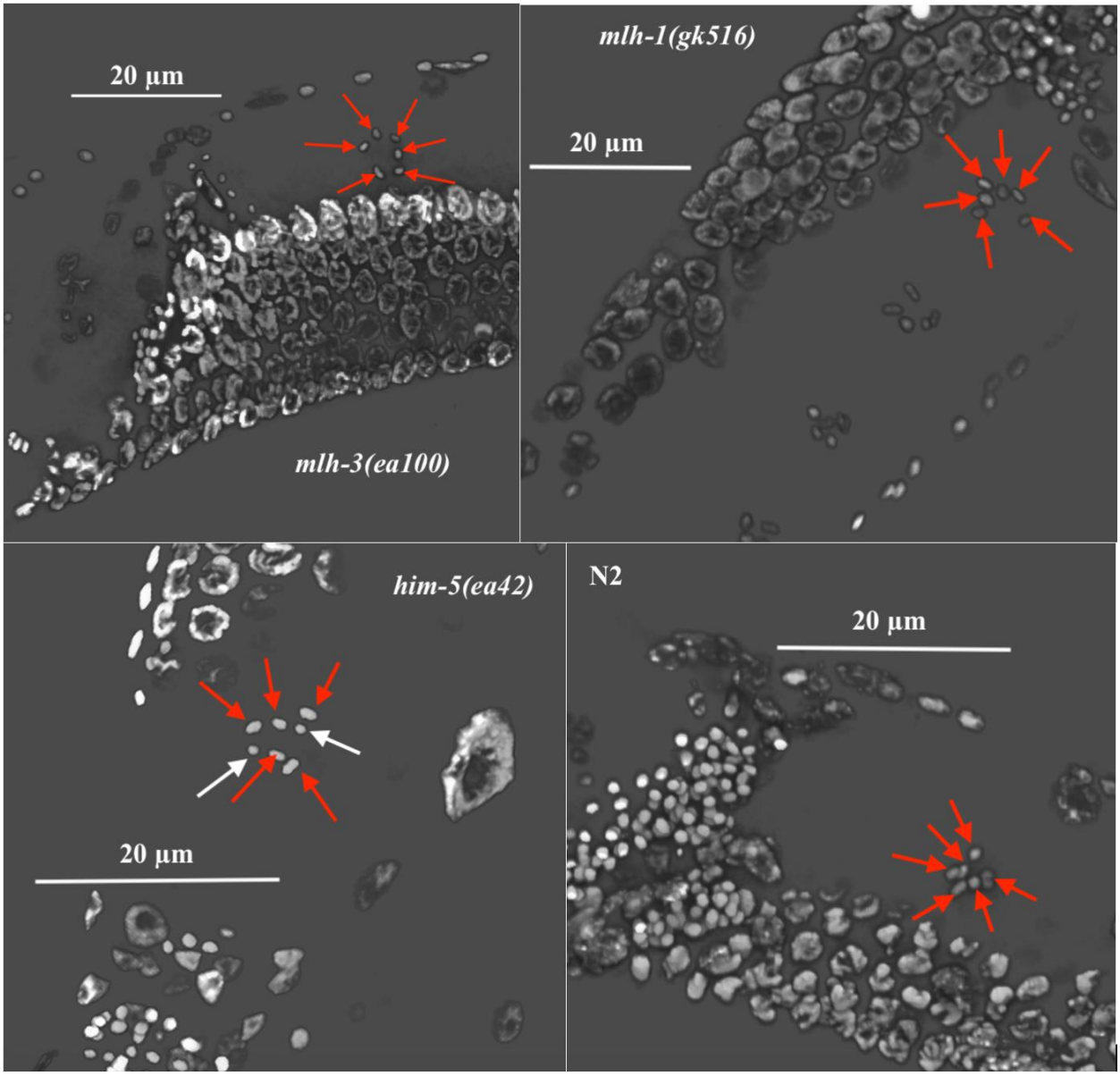

Figure 9: Confocal Imaging of Normal Single Mutants

Confocal microscopy germline images of the following stocks: N2, *mlh-1(gk516)*, and *ZK1098.3(ea100*). These represent normal counts of DAPI bodies (6) in the wild-type control, *mlh-1* KOs, and *mlh-3* KOs, respectively. Six DAPI bodies can clearly be seen in each image, indicated by the red arrows. Also included in this image is the *him-5(ea42)* stock, showing the expected DAPI body count of 7 (univalent chromosomes indicated by white arrows).

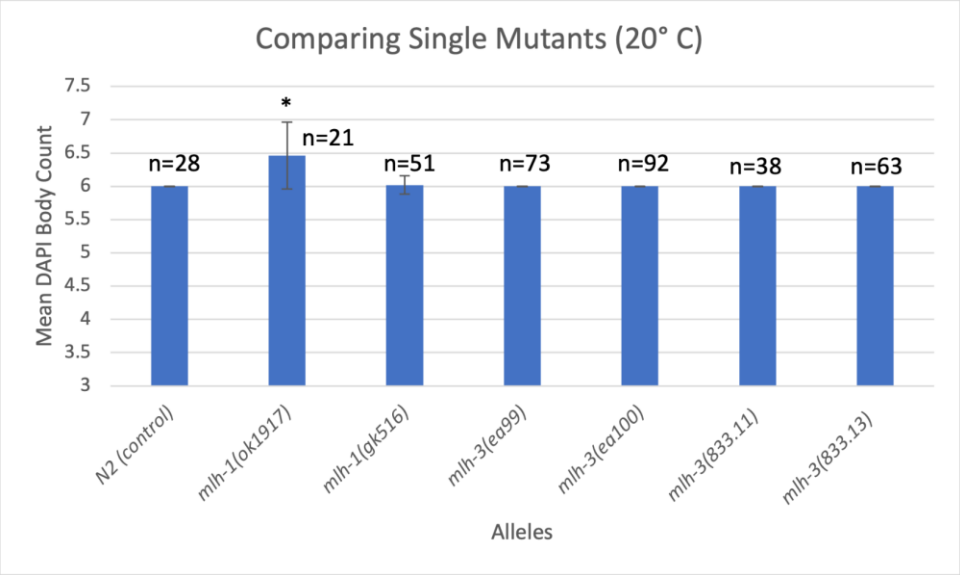

Figure 10: Mean DAPI Body Counts in Single Mutants at 20° C

Mean DAPI body count in the -1 oocytes for the following worm stocks at 20° C: N2 (wild-type), *mlh-3(ea99)* and *mlh-3(ea100)* knockouts, *mlh-1(gk516)* and *mlh-1(ok1917)* knockouts, and *mlh-3*(833.11) and *mlh-3*(833.13) (*mlh-3* homozygous worms taken from stocks that were kept balanced). Sample sizes shown are the number of germlines analyzed. There is evidently little to no difference between the DAPI body counts of these stocks, apart from the *ok1917* allele. This allele had a slightly higher mean DAPI body count (6.46) compared to the wild-type control (N2 with 6). While the difference is not large, it is statistically significant, with a p-value of 0.001 using a Student's t-test.

A similar procedure was used to determine the function of the *ZK1098.3* gene, referred to for convenience as *mlh-3*. Several KO alleles were produced. The homozygous KO alleles *ea99* and *ea100* appeared phenotypically Wild-type, growing normally. Another two alleles (*833.11* and *833.13*) were balanced over *qC1* (which has a Roller phenotype) and maintained this way. These appeared to grow in a manner consistent with *qC1*-balanced worms.

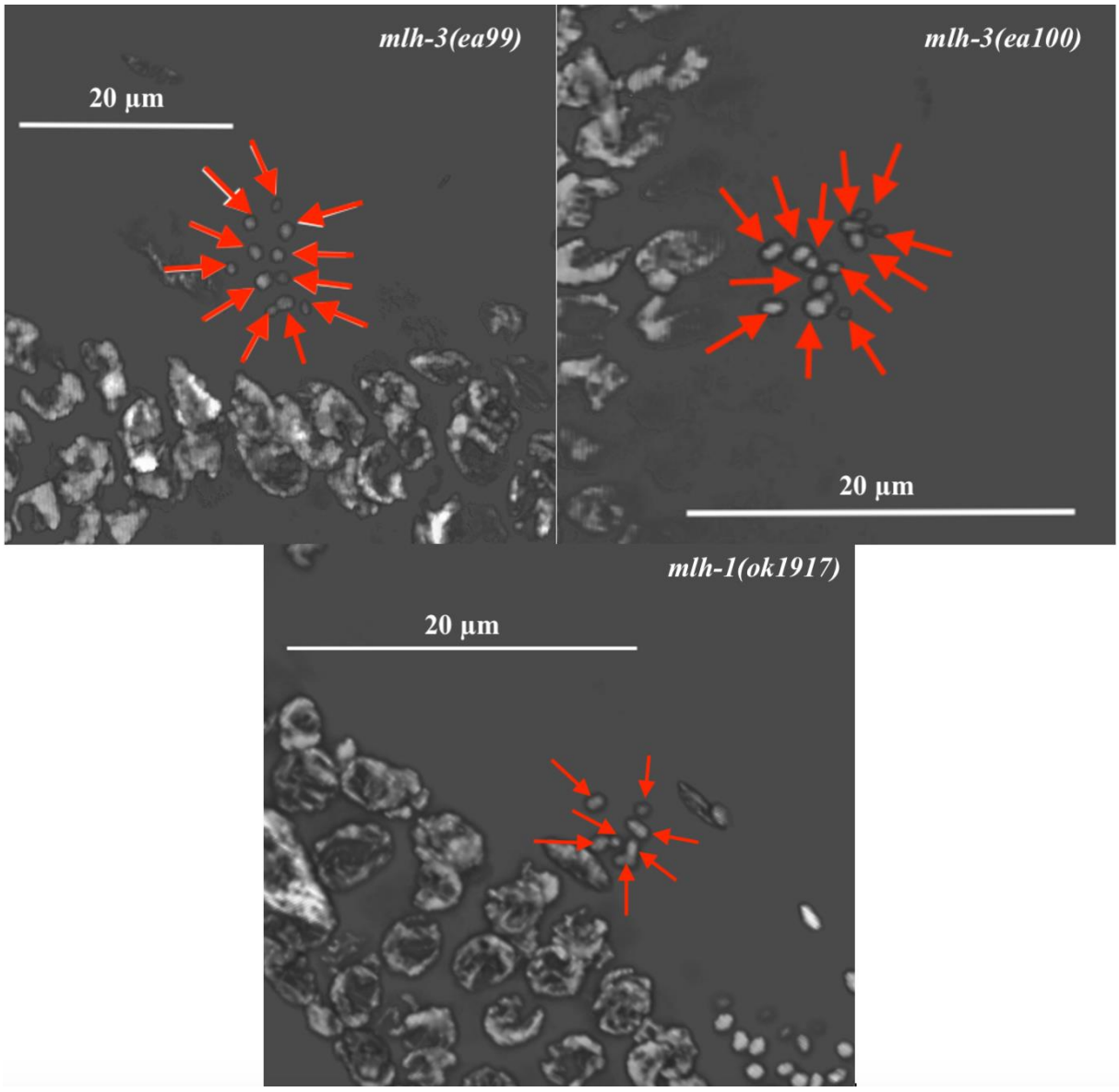

Figure 11: Confocal Imaging of Abnormal Single Mutants

Confocal microscopy germline images of *mlh-1*(*ok1917*), *mlh-3*(*ea99)* and *mlh-3(ea100)*. The *mlh-1* KO clearly displays a DAPI body count of 7, abnormal in N2 backgrounds. The *mlh-3* KOs, while normally at the expected DAPI count of 6, here display a mostly univalent phenotype, with 11 and 12 DAPI bodies shown in the *ea99* and *ea100* worms, respectively. This occurred in both germlines for one individual worm in each slide.

Non-rolling (unbalanced homozygous) worms from these stocks were stained with DAPI (19 and 34 worms for 833.11 and 833.13, respectively) and yielded 6 DAPI bodies (Figure 10). The *mlh-3(ea99)* and *mlh-3(ea100)* worms were also stained with DAPI (18 and 16 worms each, respectively) and mostly yielded 6 DAPI bodies. The exceptions were one worm per stock, in which a partially univalent phenotype with 10-12 DAPI bodies were observed. This was found in both germlines of each of the *ea99* and *ea100* outlier worms (Figure 11). To investigate the possible existence of a rare phenotype, DAPI staining of both these stocks was repeated with a larger sample size (37 and 47 worms for *ea99* and *ea100*, respectively). These worms yielded 6 DAPI bodies without variation (Figure 10).

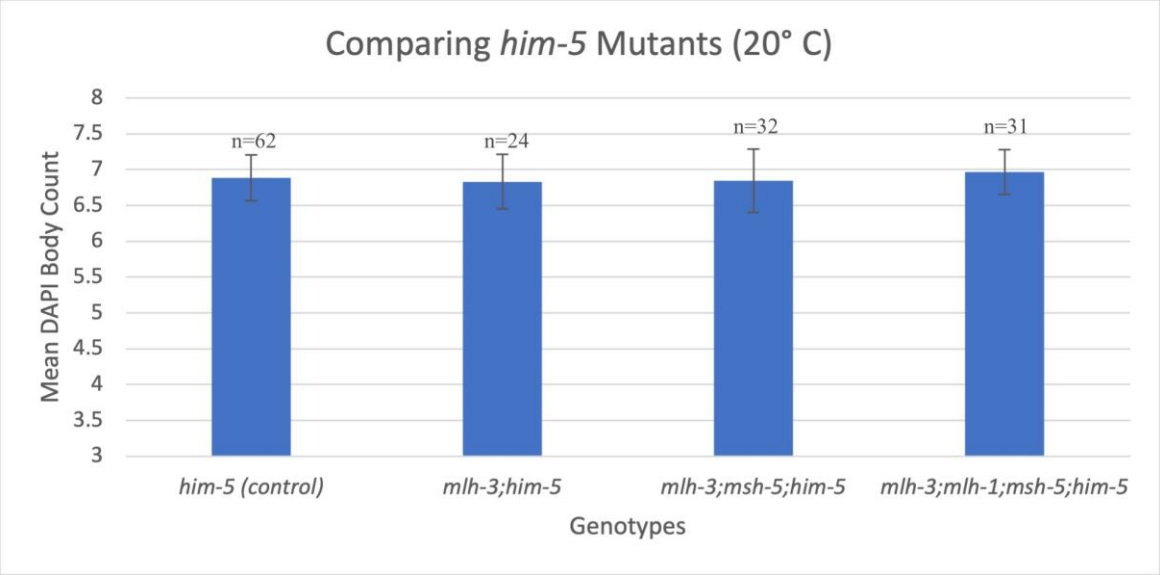

Figure 12: Mean DAPI Body Counts in *him-5* Stocks at 20° C

Mean DAPI body counts in -1 oocytes for the *him-5* background stocks: *him-5(ea42)* control, *mlh-3(ea101);him-5(ea42)*, the triple mutant *mlh-3(ea101);msh-5(ea36);him-5(ea42)*, and the quadruple mutant *mlh-3(ea101);mlh-1(ok1917);msh-5(ea36);him-5(ea42)*. The mean DAPI body counts are all extremely close at around 6.8, with no statistically significant differences between the mutants and the *him-5* control.

To test whether *ZK1098.3* has a phenotype in backgrounds sensitized to abnormal crossovers, two crosses were conducted. The first was a cross with *him-5*(*ea42*), a background with nondisjunction of the X chromosome, regularly resulting in males. The second cross was with *him-5* and *msh-5*(*ea36)*. These stocks were also stained with DAPI (15 and 19 worms, respectively). Both strains yielded DAPI body counts higher than the wild type 6. The *mlh-3;him-5* cross yielded an average of 6.8 DAPI bodies, which was not significantly different from the *him-5* control. The *mlh-3;him-5;msh-5* cross also showed a mean 6.8 DAPI bodies. This was significantly different from the *msh-5* control (Figure 13), but not from the *him-5* control (Figure 12). This might indicate that the phenotype of higher DAPI bodies in this cross is due to the *him-5* background, rather than an effect from the *mlh-3* KO.

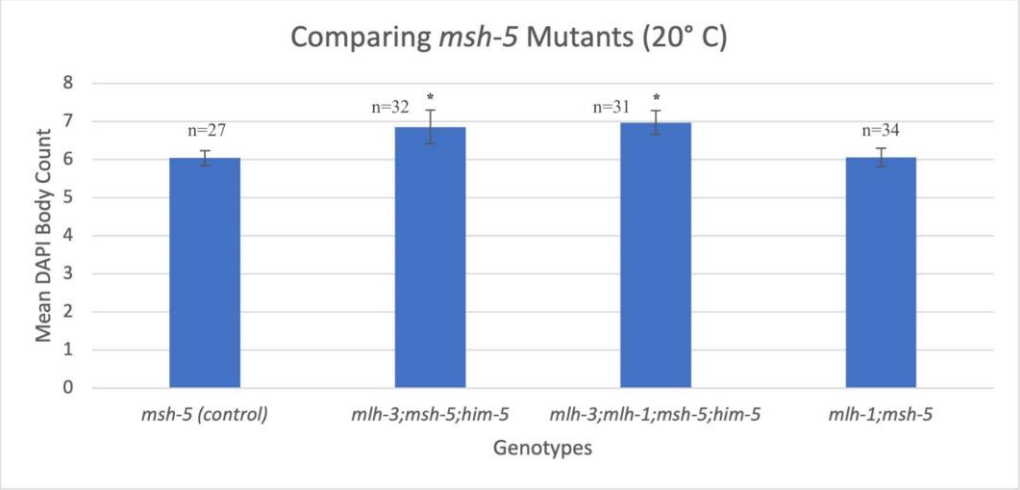

Figure 13: Mean DAPI Body Counts in *msh-5* Stocks at 20° C

Mean DAPI body count in -1 oocytes for the *msh-5* background stocks: *msh-5(ea36)* control, the double mutant *mlh-1(ok1917);msh-5(ea36)*, the triple mutant *mlh-3(ea101);him-5(ea42);msh-5(ea36)* and the quadruple mutant *mlh-3(ea101);mlh-1(ok1917);msh-5(ea36);him-5(ea42)*. The triple and quadruple mutant data are the same as Figure 12. There is a statistically significant difference between the *msh-5* control and the *mlh-3;msh-5;him-5* mutant. This difference may be due to the *him-5* background, rather than the *mlh-3*

KO. Similarly, there is a statistically significant difference between the *msh-5* stock and the quadruple mutant.

Like the *mlh-1* stocks, all *mlh-3* stocks were maintained at 25° C for two generations and DAPI stained to determine their response to heat stress. The results can be seen in Figures 14-16. None of the *mlh-3* alleles showed a statistically significant difference from the N2 control worms. Similarly, neither the *mlh-3;him-5* or the *mlh-3;msh-5;him-5* mutants showed a difference to their respective controls. This is in contrast to the results at 20° C, in which there was a significant difference between the *msh-5* control and the *mlh-3;msh-5;him-5* mutant.

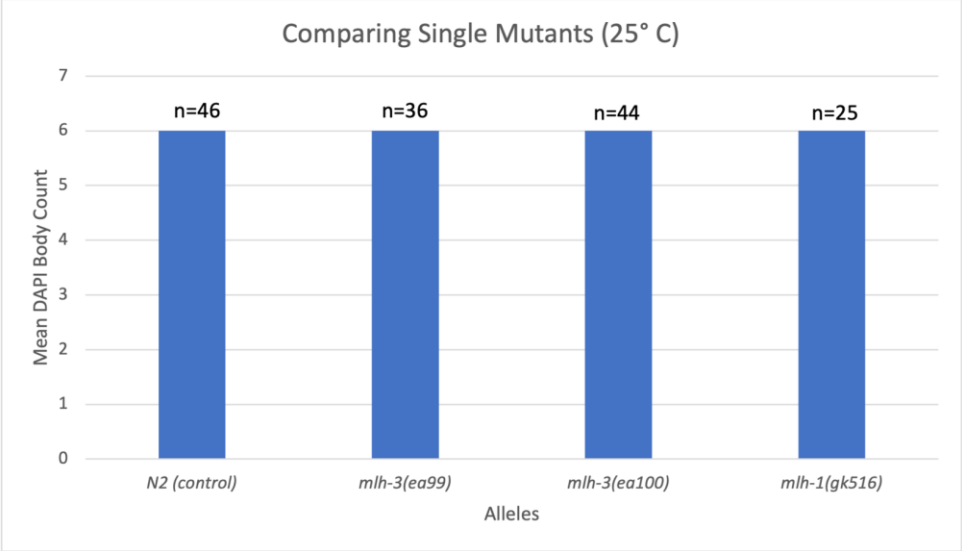

Figure 14: Mean DAPI Body Counts in Single Mutants at 25° C.

Mean DAPI body count in -1 oocytes for the following worm stocks at 25° C: N2, *mlh-3(ea99)*, *mlh-3(ea100)*, and *mlh-1(gk516)*. The *mlh-1(ok1917)* stock was omitted due to its inability to grow at this temperature. The figure clearly shows an identical DAPI body count of 6 in all germlines. No error bars are shown as all standard deviations were 0.

While there was no difference between the means for the mutants and their respective controls, there was a difference in the frequency of higher DAPI body counts. Upon review of the data, there were more instances of 8 DAPI bodies in the mutants than in either the *msh-5* or *him-5* control (Figure 17). In the triple mutant, 8 DAPI bodies were seen in roughly 16% of germlines, while in the *him-5* and *msh-5* stocks they were seen in about 2.7% and 8%, respectively. A Z-Test of proportion found a significant difference (p=0.047) between the proportions of >7 DAPI bodies in the triple mutant and *him-5* control, but not between the triple mutant and *msh-5*.

We investigated the possibility that these genes may be rescuing any phenotype caused by the other. In mammals, Mlh1 and Mlh3 act as heterodimers, and the possibility exists that, in worms, when one is knocked out the other may act to rescue the phenotype.

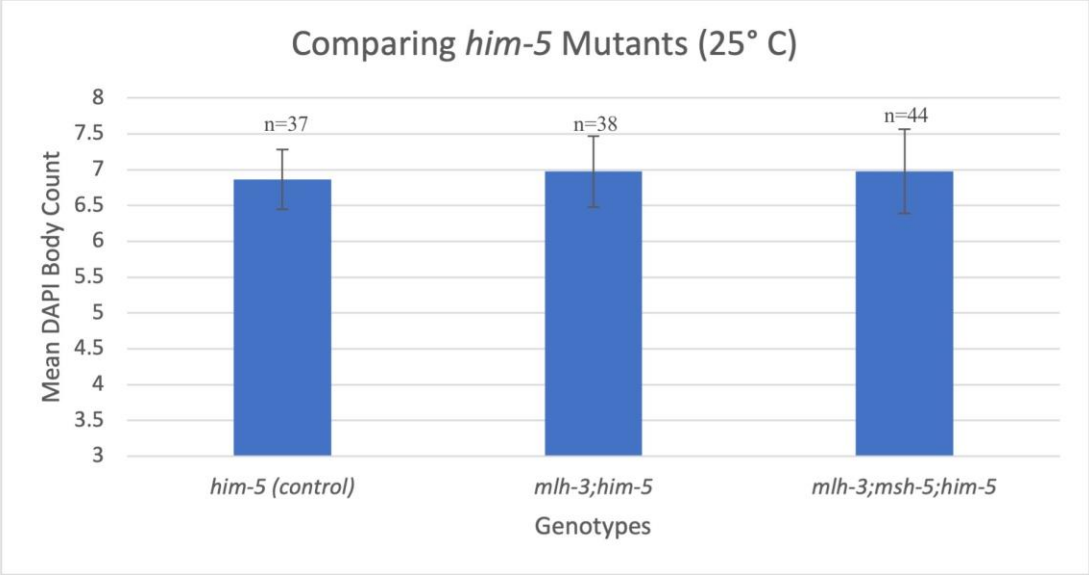

Figure 15: Mean DAPI Body Counts in *him-5* Stocks at 25° C

Mean DAPI body count in -1 oocytes for the *him-5* background stocks at 25° C: *him-5(ea42)* control, *mlh-3(ea101);him-5(ea42)*, and the triple mutant *mlh-3(ea101);msh-5(ea36);him-5(ea42)*. The figure clearly shows that all three stocks had similar DAPI body counts, with no statistically significant difference between the mutants and the *him-5* control.

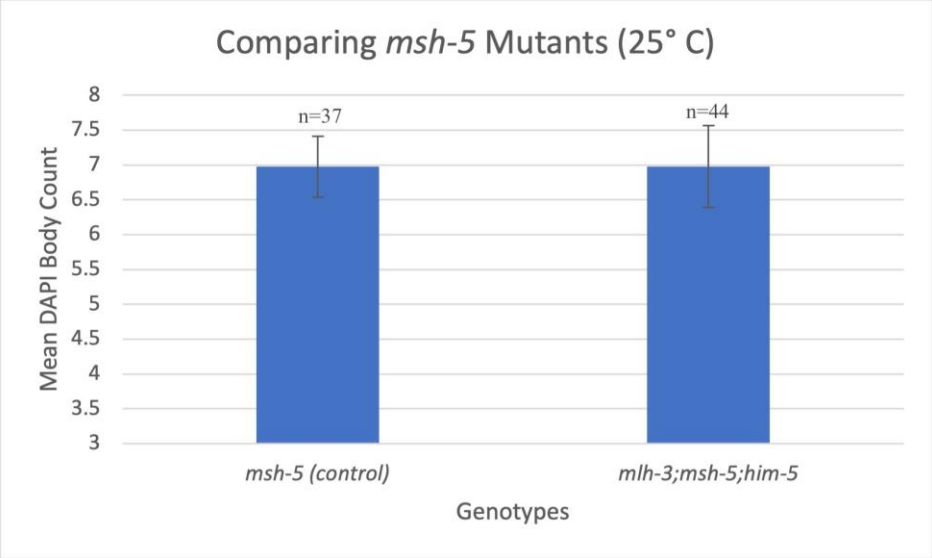

Figure 16: Mean DAPI Body Counts in *msh-5* Stocks at 25° C

Mean DAPI body count in -1 oocytes for the *msh-5* background stocks: *msh-5(ea36)* control and the triple mutant *mlh-3(ea101);msh-5(ea36);him-5(ea42)*. There was no difference between the mean DAPI body counts in each stock.

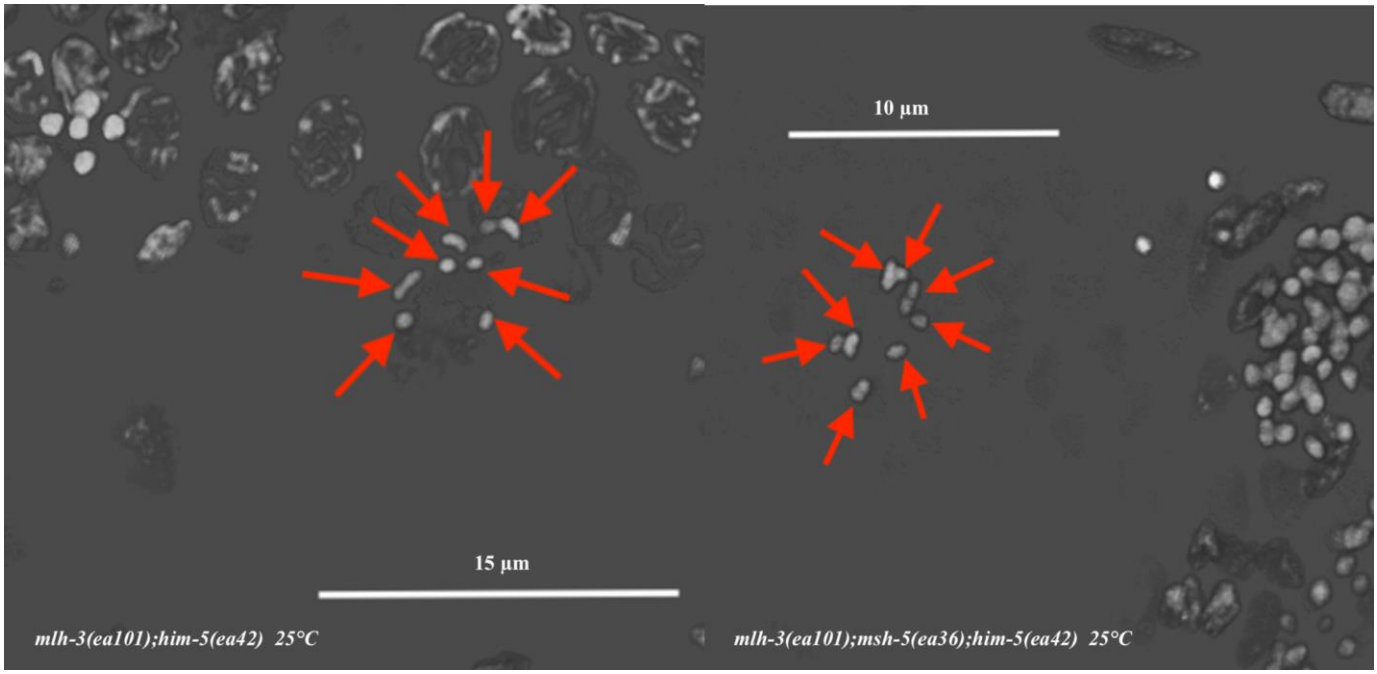

Figure 17: Confocal Imaging of Abnormal *him-5* and *him-5;msh-5* Mutants at 25° C

Abnormal DAPI body counts in *msh-5* and/or *him-5* backgrounds at 25° C. Both *mlh-3(ea101);him-5(ea42)* and *mlh-3(ea101);msh-5(ea36);him-5(ea42)* show DAPI counts of 8, as indicated by the arrows, at a higher incidence than the *him-5* or *msh-5* control.

We sought to produce a double mutant *mlh-1;mlh-3* KO by crossing balanced *mlh-3(ea101)/qC1* rolling hermaphrodites with *mlh-1(ok1917)* males. While all attempts to intentionally cross the two genes failed (these genes are linked on chromosome 3) the resulting F1 progeny (males) were used in subsequent crosses, which serendipitously yielded an *mlh-3(ea101);mlh-1(ok1917);msh-5(ea36);him-5(ea42)* quadruple mutant. This quadruple mutant showed similar results as the *mlh-3;msh-5;him-5* triple mutant, with a mean DAPI body count significantly different from the *msh-5* control, but not from the *him-5* control (Figures 12 and 13). An additional T-test comparing the triple and quadruple mutants showed no significant difference between them.

3.2 Localization of ZK1098.3

We were interested in determining the localization of the putative *mlh-3* encoded protein. To this end, we designed a CRISPR sgRNA and a repair template targeting the 5' end of the *ZK1098.3* gene (Figures 5-6), adding a new start codon and V5 tag just upstream of the original start codon. We also designed primers to target the added V5 tag sequence, allowing us to genotype the resulting offspring. The homozygotes were genotyped, purified, and sent for Sanger sequencing. The results in Figure 18 show the clear addition of a V5 tag on the 5' end of this gene.

Two V5-tagged alleles were produced, *ea102* and *ea103*. These worms appear to grow well and have Wild-type phenotypes.

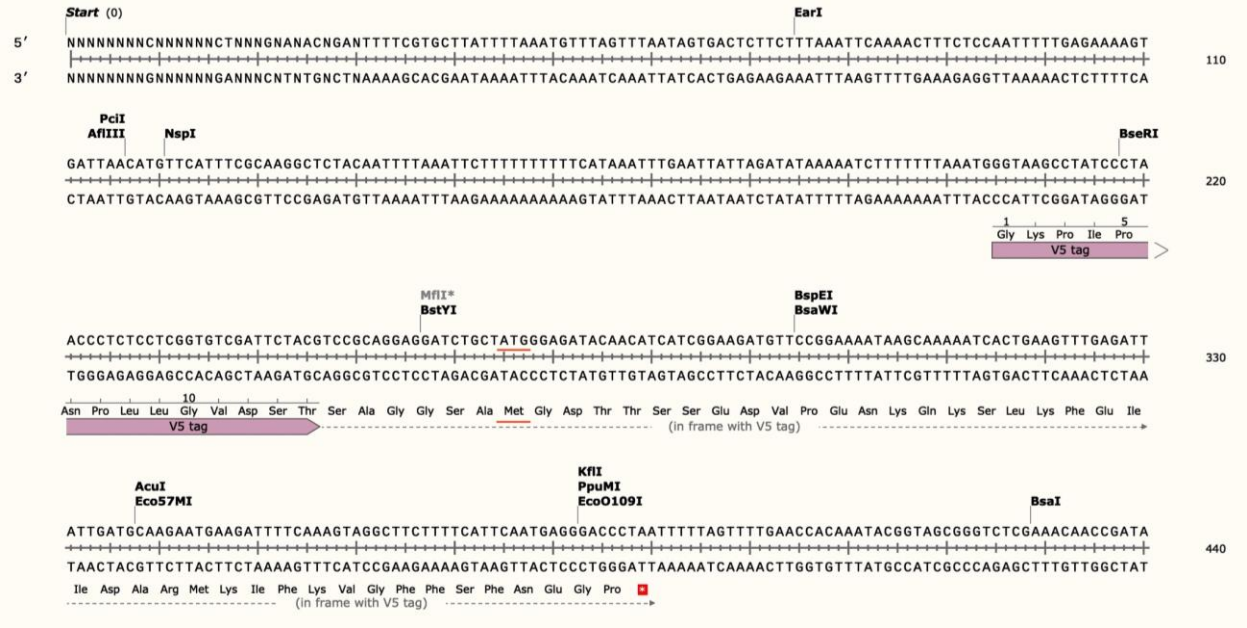

Figure 18: Sanger Sequencing Results for Alleles *V5::mlh-3(ea102)* and *V5::mlh-3(ea103)*

Variants of *ZK1098.3* with a V5 tag added to the N terminus of the protein. The V5 tag has been recognized by the software and is indicated by the purple bar. The original start codon is underlined in red, along with the corresponding methionine, indicating that the V5 tag was successfully added in frame.

One-day old adult germ lines were stained using a mouse anti-V5 antibody, rabbit anti-SYP-1 as a meiotic marker, and DAPI as a counterstain. N2 was used as a negative control. The results can be seen in Figures 19 (N2, mitotic tip), 20 (N2, pachytene region); 21 (*V5::mlh-3(ea102)*, mitotic tip), and 22 (*V5::mlh-3(ea102)*, pachytene region).

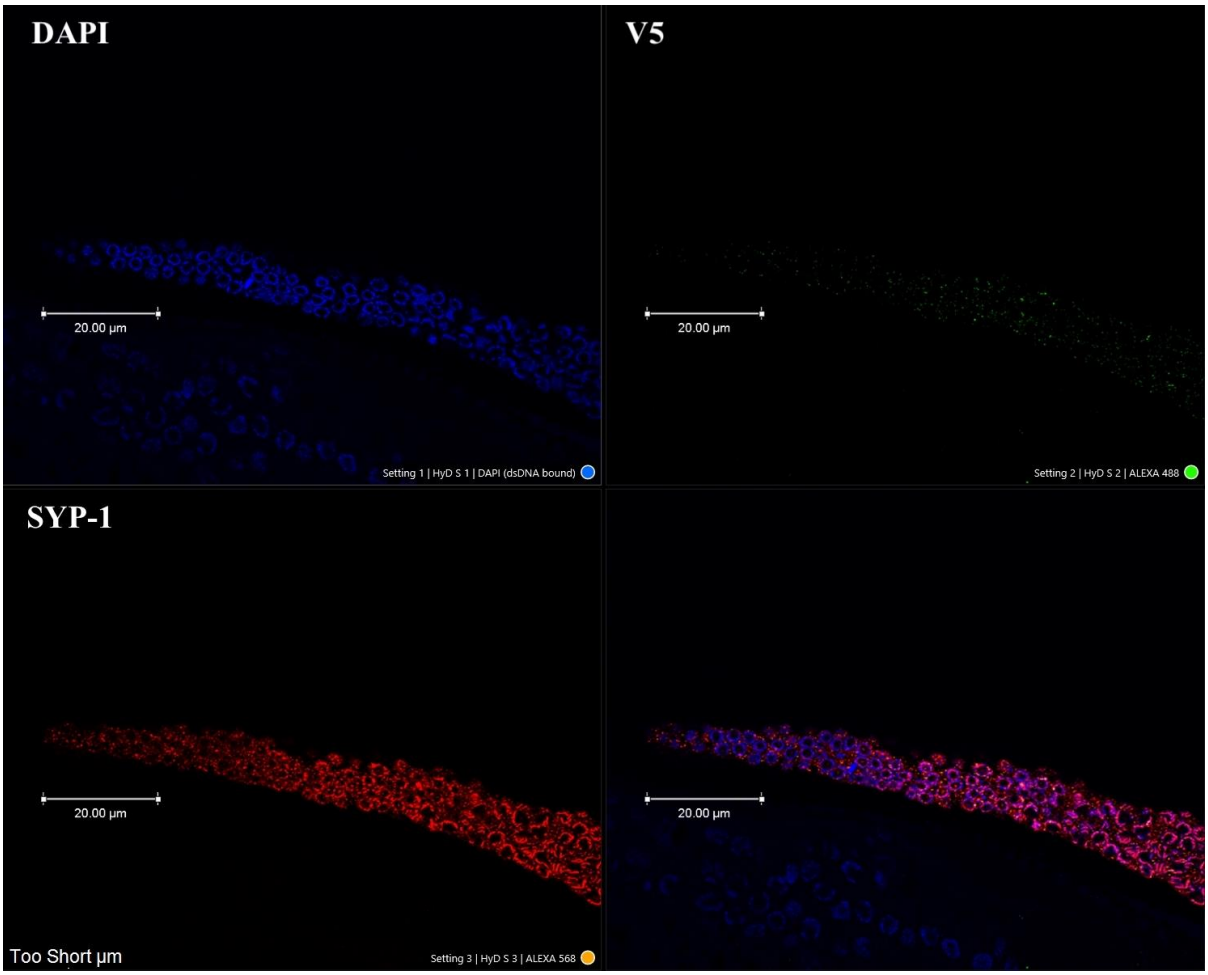

Figure 19: Confocal Imaging of N2 Germ Line Stained for V5 (Mitotic)

DAPI (top left), Rabbit-568 (anti-SYP-1, bottom left), and Mouse 488 (anti-V5, top right), taken via confocal microscopy. The bottom right quadrant shows all staining overlayed. There was no specific staining with the antibody-the mitotic portion of the germ line. SYP-1 can be seen in a faint and non-specific pattern.

The N2 controls showed little to no green coloration for V5, as was expected (Figure 19-20). The *V5::mlh-3(ea102)* and *V5::mlh-3(ea103)* germ lines showed little to no SYP-1 in the mitotic tip as expected and no V5 (Figure 21). In the meiotic pachytene region of the germ line, there is a clear presence of both SYP-1 and V5 (Figure 22). This provides evidence that *ZK1098.3* may be coding for a meiotic protein. There is a significant amount of background in the V5 staining; it is possible that a pre-adsorption step would decrease the amount of background.

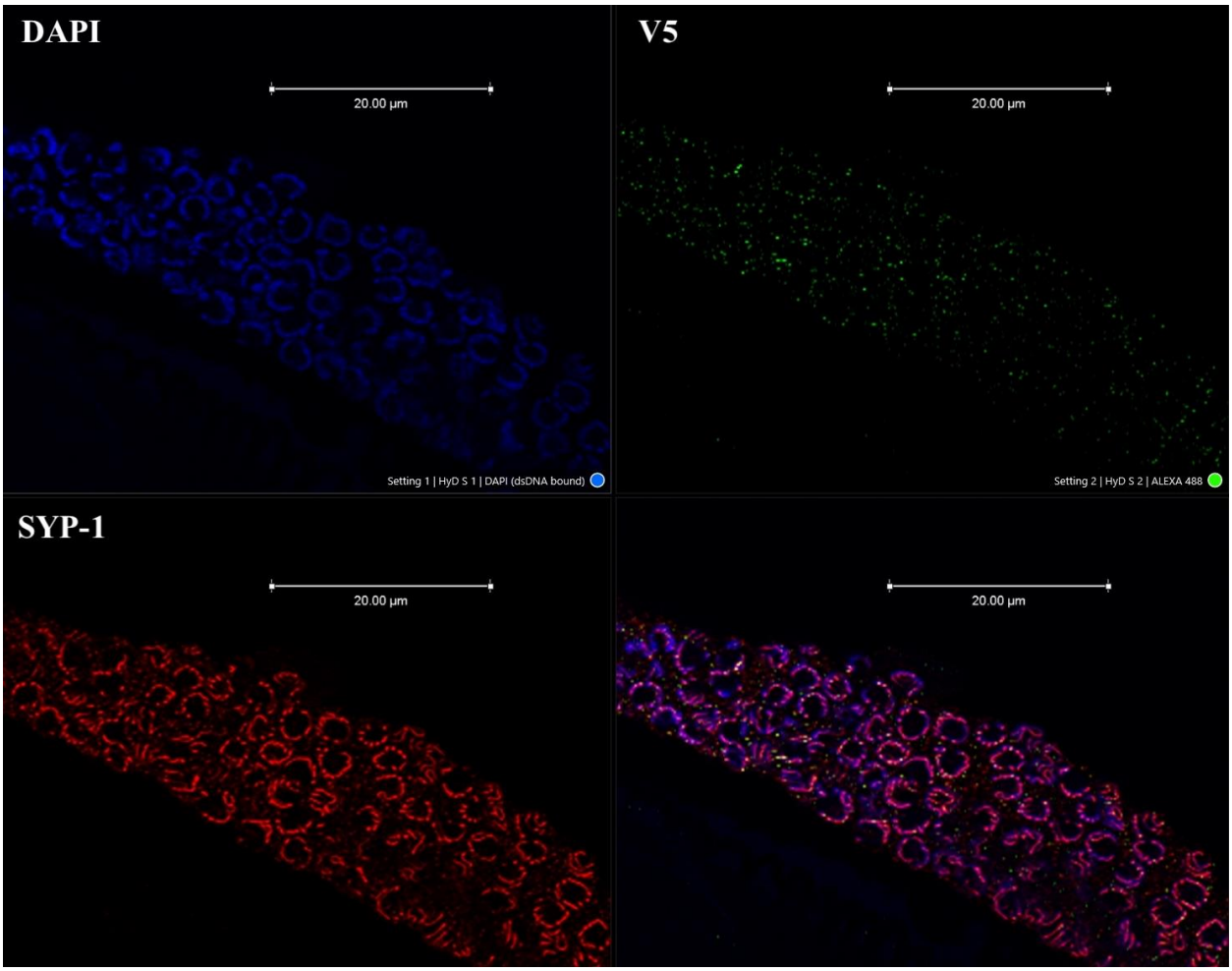

Figure 20: Confocal Imaging of N2 Germ Line Stained for V5 (Meiotic)

There is almost no V5 present in the meiotic portion of the germ line. What is visible may be background staining. SYP-1 can be seen in the pachytene oocytes.

To determine if ZK1098.3 was interacting with MLH-1 in a similar manner to Mlh1 and Mlh3 in mammals, we attempted to perform a yeast two-hybrid assay. We successfully amplified both genes from cDNA, however the Gibson assembly into the Y2H vectors was not successful. This may be due to the length of time allowed for the Gibson assembly or other factors.

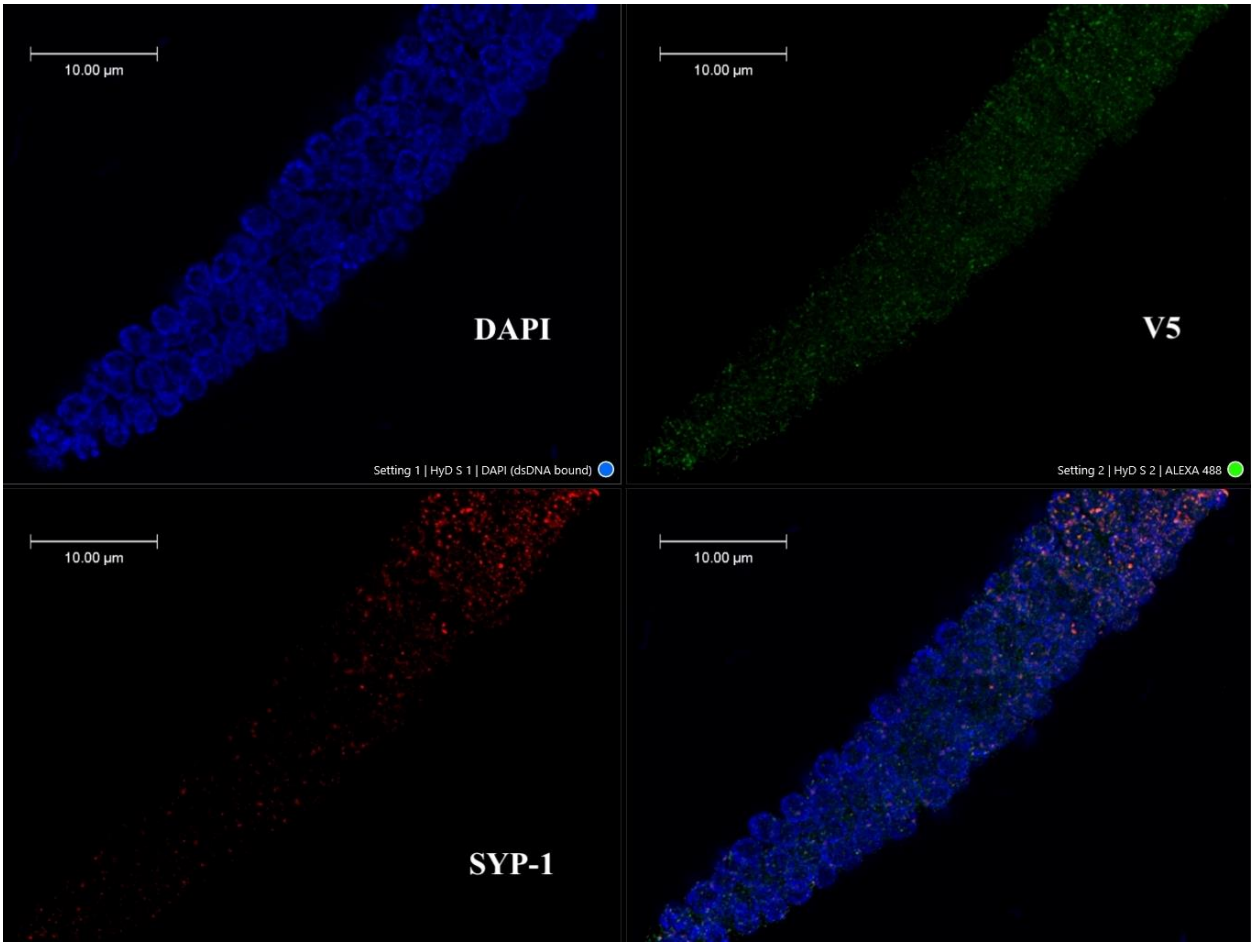

Figure 21: Confocal Imaging of *V5::mlh-3(ea102)* Mitotic Germ Line Stained for V5

Mitotic tip of an *V5::mlh-3(ea102)* worm germline, stained with DAPI (top left), Rabbit-568 (anti-SYP-1, bottom left), and Mouse 488 (anti-V5, top right), taken via confocal microscopy. There is little to no SYP-1 or V5 present.

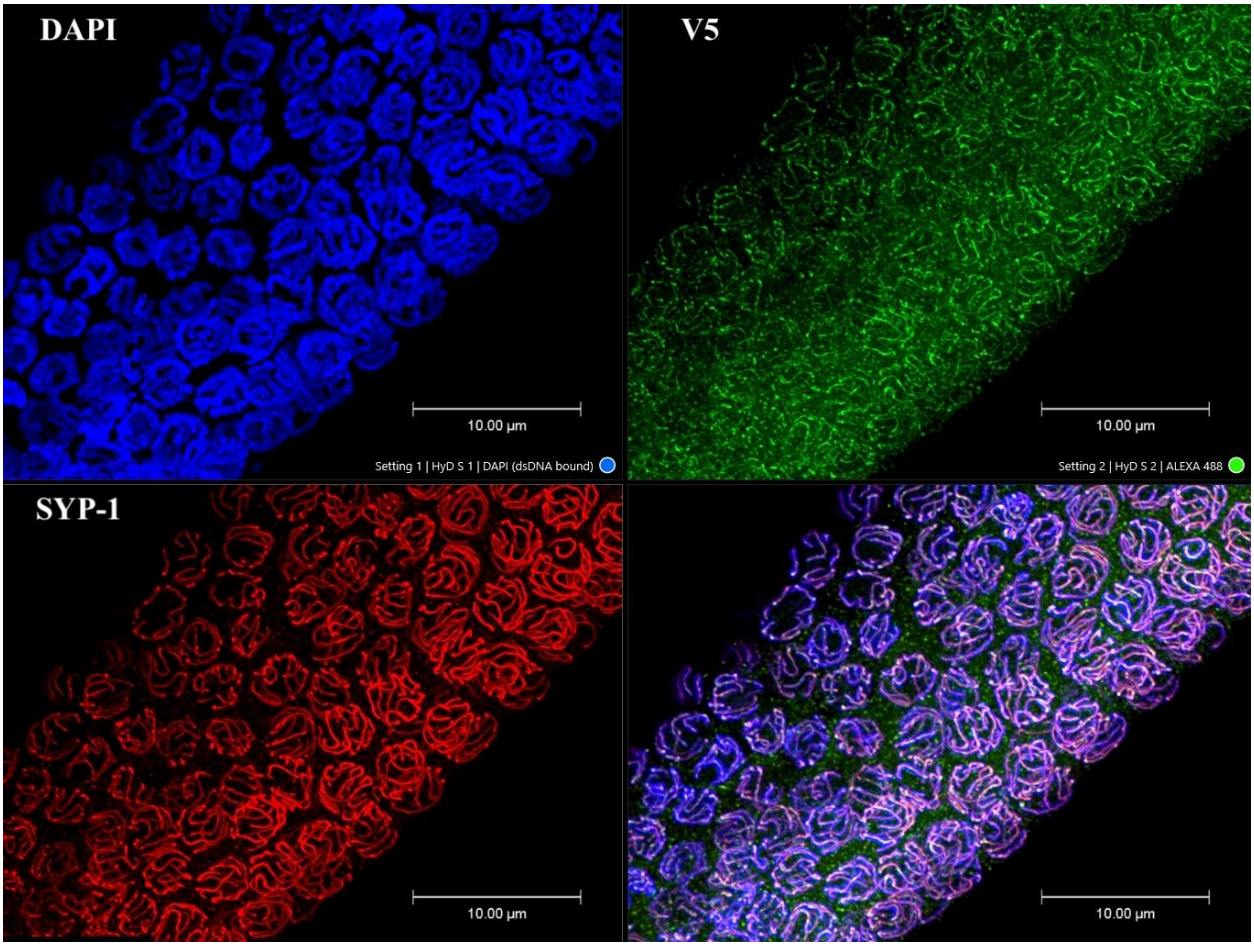

Figure 22: Confocal Imaging of *V5::mlh-3(ea102)* Pachytene Germ Line Stained for V5 DAPI (top left), Rabbit-568 (anti-SYP-1, bottom left), and Mouse 488 (anti-V5, top right), taken via confocal microscopy. The bottom right quadrant shows all staining overlayed. This shows the meiotic portion of the germline (leptotene stage). There is a clear presence of both SYP-1 and V5.

4.0 Discussion

The first goal of this project was to determine whether ZK1098.3 could be the *C. elegans* homolog of mammalian Mlh3, possibly acting as a heterodimer with worm MLH-1. One prediction of this model is that MLH-3 would be a meiotic protein. To investigate the localization of the protein, a V5 tag was added to the N-terminus. Under confocal microscopy, control worms did not stain for the presence of the tag, but modified worms stained for V5, confirming that *ZK1098.3* is actively transcribed and translated. This V5 tag revealed that the protein product of *ZK1098.3* tends to colocalize with SYP-1, a meiotic protein involved in the synaptonemal complex (MacQueen *et al*., 2002). The decreased presence of both proteins in the mitotic tip of the worm germ line, and their increased presence in the meiotic region, indicates that *ZK1098.3* is preferentially expressed in cells undergoing meiosis. This lends credibility to the idea that this locus encodes a meiotic protein. While this result is promising, the images did show a significant amount of background staining. This could mean that the V5 antibody has some non-specificity. or it could mean that there is a non-chromosomal pool of this protein that we are detecting. These results will need to be replicated and the introduction of a pre-adsorption step should decrease background and distinguish between these interpretations. By allowing the V5 antibodies to incubate with N2 worms in solution, then separating the worms from the solution, any non-specific antibodies would be removed.

We further sought a meiotic role for this gene by producing a full knockout, accomplished by a deletion of almost the entire gene. These worms thus far show no readily observable phenotype; they grow at the same rate as N2 worms, do not produce males (which are an indication of nondisjunction), and are not otherwise visibly distinguishable from controls at the normal

growth temperature of 20°C. These worms were crossed into sensitized backgrounds that give abnormal crossover numbers with the hope that, like Mlh3 in mammals which plays a role in CO resolution, these backgrounds would be more likely to see an affect. When fixed, DAPI-stained and observed under confocal spectroscopy, these KOs showed no difference in mean DAPI body count compared to their respective controls, save for two individual mutant *mlh-3* worms that presented a high number of DAPI bodies in both germ lines. This may indicate that there is a rare meiotic phenotype, but it was not observed upon repeating the staining with an increased sample size. The triple mutant (*mlh-3;msh-5;him-5*) and the quadruple mutant (*mlh-3;mlh-1;msh-5;him-5*) did present mean DAPI body counts statistically different from the *msh-5* control, but not from the *him-5*. Any difference from the *msh-5* control may then be attributable to the *him-5* background, rather than the KO. As the multiple sensitized backgrounds were an unintentional consequence of the crossing process, this would have to be reinvestigated by isolating the *him-5* and *msh-5* backgrounds from each other. Furthermore, the combination of a *ZK1098.3* KO with an *mlh-1* KO did not trigger or exacerbate any phenotype, as would be expected if either gene was acting to alleviate the loss of the other. All of these results require further confirmation by producing an *mlh-3;msh-5* double mutant, and an *mlh-3;mlh-1* double mutant free from any sensitized background.

Since heat stress can exacerbate nondisjunction and other meiotic abnormalities (Bilgir *et al*., 2013), all stocks were also maintained at 25° C, and the DAPI staining was repeated. This yielded similar results as the staining at 20° C, with the caveat that the quadruple mutant was not produced in time to be included. It will be necessary to add the quadruple mutant to this experiment to further ascertain if an *mlh-3;mlh-1* KO would behave differently at higher temperatures. Together, these data suggest that the *ZK1098.3* gene and its protein may have a minor role in

meiosis, as evidenced by confocal imaging, but not sufficiently significant to produce a meiotic phenotype, even in sensitized backgrounds under heat stress. Alternatively, the *ZK1098.3* KO may affect the proportion of abnormal DAPI body counts, rather than the average, as seen in the triple mutant *mlh-3;msh-5;him-5,* displaying a higher proportion of >7 DAPI bodies than the control. This may lead to more dead eggs and less offspring, which could be confirmed via brood size assays. In addition, the concurrent loss of *mlh-1* and *ZK1098.3* does not seem to cause a more severe meiotic defect (confirmation at 25° C needed).

To characterize the possible meiotic role of *mlh-1*, two KOs were procured. The *gk516* stock grows at similar rates to the controls but exhibits an uncoordinated phenotype. The *ok1917* stock was used instead due to its lack of a visible phenotype. However, over time this stock started developing a high incidence of males, indicating nondisjunction. These males were tested by crosses with *fog-2* worms (feminized and therefore unable to self-fertilize) and were found to be fertile. These were subsequently used in crosses to produce the quadruple mutant discussed above. Over the course of the last few months, in the course of the writing of this thesis, the health of the *ok1917* stock continued to decline. These worms now grow so slowly they do not need be passaged for two weeks and are incapable of growing at 25° C. The males have apparently become too sickly to mate, as later crosses attempted with *mlh-1* males have been unsuccessful, save one. When DAPI-stained and compared to N2 controls, these worms showed a significantly higher mean DAPI body count, consistent with their production of male offspring. In contrast, the *gk516* stock continues to appear healthy, save for their uncoordinated phenotype. They did not show a mean DAPI body count different than that of a control. This stark difference between two KOs of the same gene prompted us to genotype the *ok1917* stock for *him-5*, which would explain the production of males. The results showed the expected wild-type band, and no band at the expected

size using KO *him-5* primers, however there were other unexpected bands present. This may indicate that the *ok1917* worms have been accumulating mutations over time, which could coincidentally produce errant bands. These could be assessed by gel purification and sequencing, to determine where in the genome these bands are coming from. However, this does not explain the continued health of the *gk516* stock. *ok1917* is a deletion of exon 7 and part of exon 8 (Figure 3). This may produce a truncated transcript and protein. The *gk516* KO removes 1412 bp, starting roughly 500 bp upstream of the start codon, up to the first 900 bp of the *mlh-1* gene, including exons 1 and 2. The upstream deletion eliminates the promoter. This most likely would lead to no protein product at all. Two possible explanations immediately emerge. The first is that the truncated *ok1917* protein may have toxic effects, perhaps by interfering with DNA repair. The other explanation is that due to the method of production for these strains (non-targeted exposure to mutagens) (*C. elegans* Deletion Mutant Consortium, 2012), the *ok1917* stock carries unidentified mutations elsewhere in its genome, causing a transgenerational phenotype unrelated to *mlh-1*. Under the assumption that the *ok1917* meiotic phenotype is caused by accumulating mutations, the exact mechanism remains unclear. Mlh1 in mammals has roles in both meiosis and mismatch repair (MMR). It may be that MLH-1 does in fact have a role in meiosis, as is suggested by the DAPI body count in the *ok1917* animals. Consistent errors in meiosis may lead to the development of phenotypes in subsequent generations. An alternate explanation could be that MLH-1 has a role in MMR in *C. elegans* and that the lesions that might otherwise have been repaired start to accumulate in the mutant. The one later cross that worked (*mlh-1(ok1917);msh-5(ea36)*), showed no difference in mean DAPI body count from the control, and the sickly phenotype disappeared. Given that this is an effectively outcrossed stock of *ok1917*, it appears that whatever the direct cause of the slow growth, it is elsewhere in the genome, rather than *ok1917*

itself. A sample of *ok1917* worms were frozen at the time they were acquired. Some of these worms could be thawed and used to both produce a balanced stock and observe whether the same phenotype develops over time in the unbalanced homozygotes. To investigate the role MLH-1 may be playing in DNA repair, a newly thawed stock could be subjected to chemical mutagens or irradiated to intentionally induce DNA lesions. UV radiation, which causes thymine dimers and other individual base pair changes, may be the best option to test an MMR phenotype. A lack of ability to recover in these worms would indicate a definitive DNA repair role. As an additional method of assurance, a targeted KO of *mlh-1* could be produced via CRISPR and characterized, controlling for the possibility that the *ok1917* stock is carrying unidentified mutations from its production via mutagenesis.

These data provide preliminary evidence for the roles of *mlh-1* and *ZK1098.3*. The presence of the V5 tag under microscopy confirms *ZK1098.3* is actively expressed, rather than silent. Moreover, its localization to the meiotic portion of the germ line, along with the rare incidence of two worms with 11-12 DAPI bodies in the -1 oocyte, indicate a possible meiotic role. This role may be a minor one, as indicated by the lack of a phenotype in *ZK1098.3* KOs in various backgrounds sensitized for meiotic phenotypes. The gene *mlh-1* may also have a minor role in meiosis, as it showed an elevated mean DAPI body count. This phenotype, along with other growth and lethargy issues seen in the *ok1917* stock, may also be due to a DNA repair role or to unidentified mutations in the stock. As Mlh1 and Mlh3 act as heterodimers in mice and other mammals, ZK1098.3 cannot be confirmed as a true Mlh3 homolog until its interactions (or lack thereof) with MLH-1 are further explored, either through immunoprecipitation or a yeast two-hybrid assay. Separate *him-5* and *msh-5* background stocks could be produced, along with a double mutant *mlh-3;mlh-1*. This would allow us to analyze the phenotype of the combined KOs while

eliminating any confounding effects from the *him-5* or *msh-5* alleles. If ZK1098.3, already apparently localized at the meiotic germ line, were found to interact with *mlh-1,* it could be more confidently assumed to be an Mlh3 homolog. To elucidate the mechanism behind the conflicting phenotypes of *mlh-1(gk516)* and *mlh-1(ok1917),* the frozen *ok1917* stock could be thawed and observed over time, or a full (targeted) deletion of the *mlh-1* gene with no off-target mutations could be produced. The possible DNA repair role of *mlh-1* could be explored by induction of DNA lesions. In summation, this work provides preliminary data to elucidate the role of *mlh-1* and the uncharacterized *ZK1098.3* genes.

Bibliography

Anderson LK, Reeves A, Webb LM, Ashley T. Distribution of crossing over on mouse synaptonemal complexes using immunofluorescent localization of MLH1 protein. Genetics. 1999 Apr;151(4):1569-79. doi: 10.1093/genetics/151.4.1569. PMID: 10101178; PMCID: PMC1460565.

Barlow AL, Hultén MA. Crossing over analysis at pachytene in man. Eur J Hum Genet. 1998 Jul-Aug;6(4):350-8. doi: 10.1038/sj.ejhg.5200200. PMID: 9781043.

Bilgir C, Dombecki CR, Chen PF, Villeneuve AM, Nabeshima K. Assembly of the Synaptonemal Complex Is a Highly Temperature-Sensitive Process That Is Supported by PGL-1 During Caenorhabditis elegans Meiosis. G3 (Bethesda). 2013 Apr 9;3(4):585-595. doi: 10.1534/g3.112.005165. PMID: 23550120; PMCID: PMC3618346.

Bronner CE, Baker SM, Morrison PT, Warren G, Smith LG, Lescoe MK, Kane M, Earabino C, Lipford J, Lindblom A, *et al*. Mutation in the DNA mismatch repair gene homologue hMLH1 is associated with hereditary non-polyposis colon cancer. Nature. 1994 Mar 17;368(6468):258-61. doi: 10.1038/368258a0. PMID: 8145827.

C. elegans Deletion Mutant Consortium. large-scale screening for targeted knockouts in the Caenorhabditis elegans genome. G3 (Bethesda). 2012 Nov;2(11):1415-25. doi: 10.1534/g3.112.003830. Epub 2012 Nov 1. PMID: 23173093; PMCID: PMC3484672.

Dai J, Sanchez A, Adam C, Ranjha L, Reginato G, Chervy P, Tellier-Lebegue C, Andreani J, Guérois R, Ropars V, Le Du MH, Maloisel L, Martini E, Legrand P, Thureau A, Cejka P, Borde V, Charbonnier JB. Molecular basis of the dual role of the Mlh1-Mlh3 endonuclease in MMR and in meiotic crossover formation. Proc Natl Acad Sci U S A. 2021 Jun 8;118(23):e2022704118. doi: 10.1073/pnas.2022704118. PMID: 34088835; PMCID: PMC8201911.

Eaker S, Cobb J, Pyle A, Handel MA. Meiotic prophase abnormalities and metaphase cell death in MLH1-deficient mouse spermatocytes: insights into regulation of spermatogenic progress. Dev Biol. 2002 Sep 1;249(1):85-95. doi: 10.1006/dbio.2002.0708. PMID: 12217320.

Emmons, S.W. Male development (November 10, 2005), *WormBook*, ed. The *C. elegans* Research Community, WormBook, doi/10.1895/wormbook.1.33.1, http://www.wormbook.org.

Gruhn JR, Zielinska AP, Shukla V, Blanshard R, Capalbo A, Cimadomo D, Nikiforov D, Chan AC, Newnham LJ, Vogel I, Scarica C, Krapchev M, Taylor D, Kristensen SG, Cheng J, Ernst E, Bjørn AB, Colmorn LB, Blayney M, Elder K, Liss J, Hartshorne G, Grøndahl ML, Rienzi L, Ubaldi F, McCoy R, Lukaszuk K, Andersen CY, Schuh M, Hoffmann ER. Chromosome errors in human eggs shape natural fertility over reproductive life span.

Science. 2019 Sep 27;365(6460):1466-1469. doi: 10.1126/science.aav7321. PMID: 31604276; PMCID: PMC7212007.

Herman, R. K. Introduction to sex determiniation (December 24, 2005), *WormBook*, ed. The *C. elegans* Research Community, WormBook, doi/10.1895/wormbook.1.71.1, http://www.wormbook.org.

Hillers K.J., Jantsch V., Martinez-Perez E., Yanowitz J.L. Meiosis. (May 4, 2017), *WormBook*, ed. The *C. elegans* Research Community, WormBook, doi/10.1895/wormbook.1.178.1, http://www.wormbook.org.

Hodgkin J, Horvitz HR, Brenner S. Nondisjunction Mutants of the Nematode CAENORHABDITIS ELEGANS. Genetics. 1979 Jan;91(1):67-94. doi: 10.1093/genetics/91.1.67. PMID: 17248881; PMCID: PMC1213932.

Hunter N, Borts RH. Mlh1 is unique among mismatch repair proteins in its ability to promote crossing-over during meiosis. Genes Dev. 1997 Jun 15;11(12):1573-82. doi: 10.1101/gad.11.12.1573. PMID: 9203583.

James P, Halladay J, Craig EA. Genomic libraries and a host strain designed for highly efficient two-hybrid selection in yeast. Genetics. 1996 Dec;144(4):1425-36. doi: 10.1093/genetics/144.4.1425. PMID: 8978031; PMCID: PMC1207695.

Lim JG, Stine RR, Yanowitz JL. Domain-specific regulation of recombination in Caenorhabditis elegans in response to temperature, age and sex. Genetics. 2008 Oct;180(2):715-26. doi: 10.1534/genetics.108.090142. Epub 2008 Sep 9. PMID: 18780748; PMCID: PMC2567375.

Lipkin SM, Moens PB, Wang V, Lenzi M, Shanmugarajah D, Gilgeous A, Thomas J, Cheng J, Touchman JW, Green ED, Schwartzberg P, Collins FS, Cohen PE. Meiotic arrest and aneuploidy in MLH3-deficient mice. Nat Genet. 2002 Aug;31(4):385-90. doi: 10.1038/ng931. Epub 2002 Jul 1. PMID: 12091911.

Martín AC, Shaw P, Phillips D, Reader S, Moore G. Licensing MLH1 sites for crossover during meiosis. Nat Commun. 2014 Aug 6;5:4580. doi: 10.1038/ncomms5580. PMID: 25098240; PMCID: PMC4143925.

Macaisne N, Kessler Z, Yanowitz JL. Meiotic Double-Strand Break Proteins Influence Repair Pathway Utilization. Genetics. 2018 Nov;210(3):843-856. doi: 10.1534/genetics.118.301402. Epub 2018 Sep 21. PMID: 30242011; PMCID: PMC6218235.

Macaisne N, Touzon MS, Rajkovic A, Yanowitz JL. Modeling primary ovarian insufficiency-associated loci in C. elegans identifies novel pathogenic allele of MSH5. J Assist Reprod Genet. 2022 Jun;39(6):1255-1260. doi: 10.1007/s10815-022-02494-0. Epub 2022 Apr 18. PMID: 35437714; PMCID: PMC9174368.

MacQueen AJ, Colaiácovo MP, McDonald K, Villeneuve AM. Synapsis-dependent and -independent mechanisms stabilize homolog pairing during meiotic prophase in C. elegans. Genes Dev. 2002 Sep 15;16(18):2428-42. doi: 10.1101/gad.1011602. PMID: 12231631; PMCID: PMC187442.

Martinez-Perez E, Colaiácovo MP. Distribution of meiotic recombination events: talking to your neighbors. Curr Opin Genet Dev. 2009 Apr;19(2):105-12. doi: 10.1016/j.gde.2009.02.005. Epub 2009 Mar 26. PMID: 19328674; PMCID: PMC2729281.

Meneely PM, McGovern OL, Heinis FI, Yanowitz JL. Crossover distribution and frequency are regulated by him-5 in Caenorhabditis elegans. Genetics. 2012 Apr;190(4):1251-66. doi: 10.1534/genetics.111.137463. Epub 2012 Jan 20. PMID: 22267496; PMCID: PMC3316641.

Oh SD, Lao JP, Hwang PY, Taylor AF, Smith GR, Hunter N. BLM ortholog, Sgs1, prevents aberrant crossing-over by suppressing formation of multichromatid joint molecules. Cell. 2007 Jul 27;130(2):259-72. doi: 10.1016/j.cell.2007.05.035. PMID: 17662941; PMCID: PMC2034285.

Pannafino,G.;Alani,E. Coordinated and Independent Roles for MLH Subunits in DNA Repair. *Cells***2021**,*10*,948. https://doi.org/ 10.3390/cells100409483389/fcell.2021.695333. PMID: 34422819; PMCID: PMC8371636.

SenGupta T, Torgersen ML, Kassahun H, Vellai T, Simonsen A, Nilsen H. Base excision repair AP endonucleases and mismatch repair act together to induce checkpoint-mediated autophagy. Nat Commun. 2013;4:2674. doi: 10.1038/ncomms3674. Erratum in: Nat Commun. 2018 Mar 29;9:16206. PMID: 24154628; PMCID: PMC3826653.

Shaham, S., ed., WormBook: Methods in Cell Biology (January 02, 2006), WormBook, ed. The C. elegans Research Community, WormBook, doi/10.1895/wormbook.1.49.1, http://www.wormbook.org.

Singh P, Fragoza R, Blengini CS, Tran TN, Pannafino G, Al-Sweel N, Schimenti KJ, Schindler K, Alani EA, Yu H, Schimenti JC. Human MLH1/3 variants causing aneuploidy, pregnancy loss, and premature reproductive aging. Nat Commun. 2021 Aug 18;12(1):5005. doi: 10.1038/s41467-021-25028-1. PMID: 34408140; PMCID: PMC8373927.

Tijsterman M, Pothof J, & Plasterk RH (2002). Frequent germline mutations and somatic repeat instability in DNA mismatch-repair-deficient Caenorhabditis elegans. *Genetics, 161,* 651-60. doi:10.1093/genetics/161.2.651

World Health Organization. Infertility prevalence estimates, 1990–2021. Geneva: World Health Organization; 2023. Licence: CC BY-NC-SA 3.0 IGO.

Yokoo, R., Zawadzki, K.A., Nabeshima, K., Drake, M., Arur, S., and Villeneuve, A.M. (2012). COSA-1 reveals robust homeostasis and separable licensing and reinforcement steps governing meiotic crossovers. Cell *149,* 75–87.